The Astrophysical Journal, 601:979–999, 2004 February 1

THE ANGULAR MOMENTUM EVOLUTION OF 0.1–10 $M_\odot$ STARS FROM THE BIRTH LINE TO THE MAIN SEQUENCE

S. C. Wolff and S. E. Strom
National Optical Astronomy Observatory, 950 North Cherry Avenue, Tucson, AZ 85719; swolff@noao.edu

and

L. A. Hillenbrand
California Institute of Technology, 1200 East California Boulevard, MS 105-24, Pasadena, CA 91125
Received 2003 April 24; accepted 2003 September 30

ABSTRACT

Projected rotational velocities ($v \sin i$) have been measured for a sample of 145 stars with masses between 0.4 and greater than 10 $M_\odot$ (median mass 2.1 $M_\odot$) located in the Orion star-forming complex. These measurements have been supplemented with data from the literature for Orion stars with masses as low as 0.1 $M_\odot$. The primary finding from analysis of these data is that the upper envelope of the observed values of angular momentum per unit mass (J/M) varies as $M^{0.25}$ for stars on *convective* tracks having masses in the range $\sim$0.1 to $\sim$3 $M_\odot$. This power law extends smoothly into the domain of more massive stars (3–10 $M_\odot$), which in Orion are already on the zero-age main sequence. This result stands in sharp contrast to the properties of main-sequence stars, which show a break in the power law and a sharp decline in J/M with decreasing mass for stars with $M < 2$ $M_\odot$. A second result of our study is that this break is seen already among the pre–main-sequence stars in our Orion sample that are on *radiative* tracks, even though these stars are only a few million years old. A comparison of rotation rates seen for stars on either side of the convective-radiative boundary shows that stars do not rotate as solid bodies during the transition from convective to radiative tracks. As a preliminary demonstration of how observations can be used to constrain the processes that control early stellar angular momentum, we show that the broad trends in the data can be accounted for by simple models that posit that stars (1) lose angular momentum before they are deposited on the birth line, plausibly through star-disk interactions; (2) undergo additional braking as they evolve down their convective tracks; and (3) are subject to core-envelope decoupling during the convective-radiative transition.

Subject headings: open clusters and associations: individual (Orion) — stars: pre–main-sequence — stars: rotation

On-line material: machine-readable tables

1. INTRODUCTION

Substantial progress has been made over the past several years in characterizing the evolution of the angular momentum of low-mass ($M < 0.5$ $M_\odot$) pre–main-sequence (PMS) stars as they evolve toward the main sequence (e.g., Herbst, Bailer-Jones, & Mundt 2001; Rebull 2001 and references therein). In this paper, we report new observations of angular momentum in intermediate-mass PMS stars in the mass range 0.4–3 $M_\odot$ and zero-age main-sequence (ZAMS) stars for a coeval population at masses greater than 4 $M_\odot$, ranging up to greater than 10 $M_\odot$. Our first goal is to establish for stars in this mass range the values of angular momentum (J) for stars with ages of less than 1 Myr, which we will take as an estimate of the initial angular momentum. Our second goal is to compare these values with older stars to examine how angular momentum changes as a function of time.

To place our observational results in context, we adopt what has become the standard framework for early stellar evolution, i.e., that stars acquire a significant fraction of their final mass through rapid accretion via disks. If protostars end the phase of rapid accretion quickly, that is, on a timescale that is short relative to the timescale for contraction, then it is possible to derive a relationship between mass and radius and to use this relationship to define a locus of points in the temperature-luminosity plane where the rapid accretion stops and stars become visible and begin their quasi-static contraction to the main sequence. This locus is the birth line (Stahler 1983). Stars may then continue to accrete material at a low rate as they evolve from the birth line down convective tracks.

Stars that form as a result of accretion of high angular momentum material through a disk should in principle be rotating at nearly the breakup speed (Durisen et al. 1989), but the typical rotational velocities of the youngest visible stars are instead observed to fall an order of magnitude or so below this critical velocity (Stauffer & Hartmann 1986; Rhode, Herbst, & Mathieu 2001). The low rotational velocities have been explained by positing that stars are locked to their surrounding disks via magnetic fields and that the disk applies a braking torque (Uchida & Shibata 1984; Königl 1991; Shu et al. 1994). Therefore, a second key element of the overall framework is that accreting protostars lose angular momentum through interaction with an accretion disk before they arrive at the birth line.

In order to account for subsequent changes in angular momentum and surface rotation as PMS stars evolve from the birth line onto the main sequence, a number of additional factors must be taken into account: (1) continued loss of angular momentum via coupling to disks at the lower accretion rates characteristic of T Tauri stars, (2) changes in the moment

of inertia as a result of changes in stellar radius and internal structure, and (3) possible decoupling within the star between rotation of its core and rotation of its envelope.

In the sections that follow, we first describe observations designed to determine the angular momenta of extremely young intermediate-mass stars. These data provide an estimate of the initial angular momentum as a function of mass. We then compare these observations with older stars and with the above theoretical framework in order to learn whether these basic ideas can account for the observed changes in stellar rotation as a function of time and mass.

2. OBSERVATIONS

2.1. *Sample Selection*

An ideal sample for our purposes is one that (1) contains a statistically significant number of young stars having $M > 0.5\ M_{\odot}$ and (2) includes objects born in multiple star-forming episodes so that stars of identical mass can be observed in a variety of evolutionary states. The Orion OB association is one of the nearest star-forming regions that satisfy these criteria. The ages of the stars in this region range from less than 1 to 10 Myr (Walker 1969; Warren & Hesser 1978; Brown, de Geus, & de Zeeuw 1994; McNamara et al. 1989).

A sample of stars brighter than magnitude $B = 14$ with proper-motion membership probabilities larger than 50% was selected from the studies of McNamara et al. (1989), van Altena et al. (1988), and Jones & Walker (1988). This sample is spread over a diameter of about $2\overset{\circ}{.}75$ located within the Orion Ic/Id association.

For each sample object, we require photometric and spectroscopic data sufficient to determine (1) the star's location in the H-R diagram; (2) its projected rotational velocity; (3) whether or not the star is surrounded by a circumstellar accretion disk, which might "lock" a star to a fixed rotation period (e.g., Königl 1991); and (4) whether or not a star is a short-period spectroscopic binary in which each member's rotational velocity could be tidally locked to the orbital velocity.

We obtained spectra of resolution and wavelength coverage sufficient to determine spectral types and also to measure projected rotational and radial velocity values. We also obtained near-infrared photometry (*JHK*), which in combination with derived spectral types and extant optical photometry enables estimates of excess emission above photospheric levels and serves as a diagnostic of circumstellar accretion disks. We culled from the literature optical (*UBVI*) photometry, as well as spectral types and $v \sin i$, for a few stars for which we obtained IR photometry but no spectroscopy.

The databases for our sample are given in Tables 1 and 2. In general, Table 1 includes the observations, while Table 2 includes such derived quantities as visual extinction (A_V), effective temperature ($T_{\rm eff}$), luminosity ($L_{\rm bol}$), radius (R), moment of inertia (I), mass (M), age (A), and infrared excess [$\Delta(H-K)$]. The entries in the tables are described in the sections that follow.

2.2. *Spectroscopic Measurements*

High-resolution ($R \sim 20,000$) spectroscopic data were obtained in 1992 November and 1993 January with the Hydra multiobject spectrograph mounted on the KPNO 4 m telescope. The "heart of Hydra" is a robotic fiber-positioning device that permits the observer to locate as many as 97 fibers at locations within a $45'$ field to subarcsecond precision. Typically, we were able to optimize fiber placements to enable simultaneous observation of 40–60 object spectra and 30–40 sky spectra. Priority in the assignment of fibers was given to Orion stars that had been shown to have excess emission at near-infrared wavelengths by our *JHK* photometry. Two echelle settings with a spectral range of $\sim$150 Å were used. The first was centered at λ4450 and included He I λ4471 and Mg II λ4481. The second was centered at λ4861 and included the Hβ line. Spectra centered on the He/Mg region enable rotational velocity measurements for stars spanning a wide range in spectral type, while those centered on Hβ provide a complementary measure of rotational velocity for stars of type A5 and later.

Our observing strategy was to obtain the He/Mg and the Hβ settings on different nights of the observing runs in order to enable the identification of spectroscopic binaries via radial velocity variations. On each night, the data were obtained in two steps, first by taking a series of exposures with the telescope and fibers aligned on our target positions and then by offsetting the telescope by $\sim 5''$ to obtain a "sky" exposure. This procedure (as opposed to the more standard practice of achieving sky subtractions by averaging several "sky" fibers) was necessitated by the large and spatially variable background of the Orion Nebula, which was assessed empirically via comparison between sky fibers from "on-target" and "offset" telescope positions.

We also obtained spectra of a grid of relatively bright stars to be used as rotational velocity standards. For spectral types later than A0 these were stars in the Pleiades cluster (Anderson, Stoeckly, & Kraft 1966) and field stars (Soderblom, Pendleton, & Pallavicini 1989) for which accurate rotational velocities are known. For hotter stars, the standards were taken from Slettebak et al. (1975).

The Hydra data were reduced with the IRAF script DOHYDRA developed by F. Valdes at NOAO. The first step in the reduction procedure requires removal of a low spatial frequency pattern, which is superposed on the spectra and results from the summed contributions of light emerging from the object and sky fibers and then scattered by the optical train. The scattered light background is removed using the IRAF task APSCATTER by (1) measuring its contribution outside the regions occupied by object and sky spectra, (2) fitting a two-dimensional surface to the scattered light pattern, and (3) subtracting the surface fit.

The next steps involve extraction of the object and sky spectra and wavelength calibration. The latter step is accomplished by extracting spectra of a ThAr arc source taken with the same fiber configuration used to record stellar and sky spectra and deriving individual dispersion solutions for the arc spectrum corresponding to each fiber. The resulting wavelength versus pixel fits are then applied to the intensity/pixel relationship for the corresponding object or sky spectrum. The final step requires subtraction of a sky spectrum from each object spectrum. Typical sky corrections were less than 10% of the stellar signal even for the faintest stars in our sample. The resulting typical signal-to-noise ratio (S/N) per resolution element is between 30 (for the faintest stars) and 150 (for the brightest stars).

Spectral types were derived via comparison with our grid of spectral standards. For stars of types mid-G and earlier, our classifications enable placement on a standard sequence to within ± 1 subclass. For stars of later type (which are also fainter on average), the uncertainties are somewhat higher, perhaps ± 2 subclasses on average, because of the difficulties

inherent in classifying spectra for which the number of decisive classification features contained within the relatively short wavelength span sampled is small and for which the S/N is modest (30/1).

Rotational and radial velocities were measured with a cross-correlation technique. By cross-correlating an object spectrum of unknown line width with that of a template spectrum of known line width (usually taken to be a slowly rotating star with $v \sin i$ smaller than the instrumental resolution), one can measure the width of the resulting cross-correlation function. The width of this function is proportional to broadening introduced by rotation and thus to $v \sin i$. Tonry & Davis (1979) originally developed this technique in an astronomical context in order to derive velocity dispersions in galaxies. The IRAF RV package contains the script FXCOR, which incorporates the Tonry and Davis formalism.

Our observations span a very wide temperature range, and the appearance and particularly the density of absorption lines change dramatically over this spectral range. Therefore, we have used spectral type–dependent techniques to estimate apparent rotational velocities.

For stars with spectral types earlier than A5, for which the number of lines contained within our spectral windows is too small to enable accurate $v \sin i$ and v(radial) measures from cross-correlation techniques, projected rotational velocities were obtained via visual comparison with artificially broadened slowly rotating templates of comparable spectral types (from O9 to A5) and crosschecking with standard stars having known rotational velocity. Radial velocities were obtained from measurements of line centroids and then placed on the internal HYDRA system for the later type stars from comparison of radial velocity values derived from line centroids and cross-correlation peak measurements for a selection of stars in the spectral type range A5–F5. Our estimated uncertainty in $v \sin i$ for stars A5 and earlier is 50 km s^{-1}, for typical $v \sin i$ values of 100–200 km s^{-1}. Our estimated uncertainty in v(radial) is 10 km s^{-1}. To be listed as a candidate spectroscopic binary, a star with spectral type A5 or earlier must have a velocity that differs by 20 km s^{-1} from the cluster mean.

For stars later than A5, the first step in our procedure was to fit a function to the stellar continuum level and subtract this function from both the object and the template spectra. We then filtered the object and template spectra with a function tailored to reject low spectral frequencies (i.e., contributions to the power spectrum deriving from broad blends of atomic or molecular features). For the F, G, and K stars in our sample for which the rotational velocities were typically $v \sin i < 100$ km s^{-1}, we rejected frequencies corresponding to features with widths 200 km s^{-1} or greater; the expectation that the line widths were less than 200 km s^{-1} was verified by visual inspection of the spectra. For the A stars in our sample, we used a filter that rejected only those features with widths 400 km s^{-1} or greater. The object and template spectra were then cross-correlated. By fitting a Gaussian to the resulting function, we determined both its peak (which measures the relative radial velocity of object and template stars) and its FWHM (which provides a measure of the rotational velocity of the object). This procedure closely follows that described by Hartmann et al. (1986), who used a similar technique to derive rotational velocities for solar-type PMS stars.

In practice, we chose a template star, SAO 217014 (G5 V; $v \sin i < 5$ km s^{-1}), which was used as the cross-correlation template for all object stars with spectral types F0–K5. For stars with two or more independently measured spectra, the agreement between the FWHM of the Gaussians that best fit the cross-correlation function is generally better than 5% for FWHM < 60 km s^{-1} and better than 10% for broader lines.

The relationship between FWHM and projected rotational velocity for the stars later than A5 is established via comparison with published $v \sin i$ values for the Pleiades stars included in our Hydra sample. Figure 1 shows the relationship between FWHM and $v \sin i$ for the 34 stars used to establish the functional relationship between these quantities. With the exception of three obviously discrepant points, the scatter about the adopted calibration curve is less than 10% at all values of $v \sin i$. We estimate typical precision of 20 and 3 km s^{-1} for rotational and radial velocities, respectively, for stars of spectral type A5 and later.

Our measurements of $v \sin i$ are listed in Table 1 along with previous measurements by other authors. A number of the stars have been measured in other studies, but in order to make the data set as homogenous as possible, we have adopted (see Table 2) our own measurements of $v \sin i$ rather than averaging our measurements with those in the literature. We have, however, supplemented our data by using values of $v \sin i$ from the literature for a few stars for which we had photometry (see below) but no spectroscopy. In adopting values from the literature we have confined ourselves to a few large data sets (see the notes in Table 2) that had some stars in common with the current survey and for which there was good agreement with our measurements.

Our data set also permits a search for spectroscopic binaries. Because Hydra records spectra for a large sample of cluster members simultaneously, we can compare the velocities derived from the location of the cross-correlation peak for each star with the mean velocity for all stars in a given Hydra exposure. We tested this procedure for our Pleiades cluster standard stars of spectral types A5 and later and find that the scatter about the mean is typically ± 2.5 km s^{-1} (1 σ) for these high-S/N spectra. For our Orion data, the scatter is ± 4 km s^{-1}. Stars in our sample with spectral types A5 and later that deviate by more than 2 σ (8 km s^{-1}) from the mean in any of our Orion sample Hydra exposures are tagged in column (15) of Table 1 as "candidate " spectroscopic binaries, along with the observed range in velocity in kilometers per second. We emphasize that confirmation of candidates as true spectroscopic binaries (as opposed to field star interlopers sharing the proper motion but not the radial velocity of the Orion association) will require additional observations.

The 12 candidate binaries include convective as well as radiative stars and both high- and low-mass objects. The binaries do not occupy a special location in any of the diagrams relating angular momentum to mass. Accordingly, we do not treat them separately in the discussion that follows.

2.3. *Infrared Observations*

In planning our overall program, we believed that IR measurements might lead to discovery of a significant number of disks around the stars in our sample. The quantity $\Delta(H-K)$, the difference between reddening-corrected $H-K$ color and underlying photospheric color, provides a strong discriminant between disked and diskless stars (Hillenbrand et al. 1992; Edwards et al. 1993; L. A. Hillenbrand et al. 2004, in preparation).

Near-infrared (*JHK*) observations were obtained for several hundred stars in the Orion Ic/Id association that met the proper-motion criteria defined above. The observations were made in 1991 November and December with the OTTO

TABLE 1

OBSERVED PARAMETERS

Parenago No.[a] (1)	V (mag) (2)	$B-V$ (mag) (3)	$U-B$ (mag) (4)	UBV Ref.[b] (5)	I_C (mag) (6)	$V-I_C$ (mag) (7)	VI Ref.[c] (8)	J (mag) (9)	$J-H$ (mag) (10)	$H-K$ (mag) (11)	JHK Ref.[d] (12)	Sp. Type (13)	Sp. Type Ref.[e] (14)	$v \sin i$[f] (km s^{-1}) (15)	$v \sin i$ Ref.[g] (16)	Brun No.[h] (17)	HD No. (18)	HR No. (19)	Group (20)
82.....	7.97	−0.04	−0.35	2	7.98	−0.01		...	...	...		B8–B9, B9	10, 11	200	8		36120		C
378.....	8.65	−0.06	−0.38	2	8.75	−0.10		8.79	−0.03	−0.04	1	B8–A0, A0	10, 11	15	8		36234		C
597.....	8.18	0.05	−0.04	2	8.07	0.11		...	...	...		B9	10, 11	25	8		36366		C
679.....	6.22	−0.18	−0.75	2	...	...		6.66	−0.06	−0.07	1	B2.5, B2	12, 7, 11	15, 10, 40	4, 10, 12		36430	1848	C
854.....	7.69	−0.08	−0.45	2	7.74	−0.05		7.88	−0.03	−0.04	1	B5.5, B8	12, 11	190	8		36541		C
908.....	8.81	−0.04	−0.22	2	8.85	−0.04		8.89	−0.01	−0.04	1	B8–B9	10, 11	135	8		36559		C
1044.....	7.69	0.01	−0.65	1	...	...		7.58	0.01	−0.01	1	B2–B3	1, 3, 11	< 50	1	25	36629		C1
1049.....	11.87	1.60	1.54	1	...	...		8.78	0.05	0.89	1	K5–K7	1	4–20 (SB:50)	1	29			C1
1076.....	12.60	0.47	...	5	...	...		10.26	0.61	0.45	1	K1	9	22	11	42			C
1097.....	8.63	−0.04	−0.08	1	...	...		8.62	0.06	0.00	1	B8, B9	3, 11	150	8	50	36655		C
1126.....	8.98	0.01	−0.06	1	...	...		8.97	0.00	−0.03	1	B9–A0	1, 3, 11	80	1	62	36670		C1
1179.....	11.52	0.53	−0.02	1	...	...		10.42	0.24	0.03	1	F5, F8	1, 3	114	1	89			C1
1270.....	12.11	0.92	0.68	1	11.01	1.10	4	10.28	0.58	0.27	1	K1	9	16	11	141			C
1319.....	12.58	1.11	0.53	1	...	...		10.29	0.54	0.15	1	F5–G0, K0	1, 4	187, 279	1, 6	166			C3
1322.....	11.70	0.85	0.33	1	10.76	0.94	4	10.12	0.40	0.10	1	G8	1	70	1	168			C2
1326.....	11.34	1.46	1.31	2	...	...		8.45	0.64	0.17	1	K5	1	4–20 (SB:13)	1	172			C1
1345.....	12.00	1.26	...	5	...	...		9.19	0.70	0.17	1	K5	1	4–20	1				C1
1360.....	13.81	0.94	0.42	1	...	...		...	...	...		G8	4	15	3	182			C2
1374.....	10.31	0.56	0.10	4	9.66	0.65	4	9.14	0.27	0.04	1	F6	1	77	1	203			D1
1391.....	10.63	0.49	0.04	1	10.11	0.51	2	9.68	0.23	0.06	1	F7	1, 3	15 (SB:30)	1	211			C3
1393.....	12.16	0.78	0.37	4	11.08	1.04	1	10.32	0.53	0.08	2	K0, G6	1, 2	10	3, 1	213			D1
1394.....	10.29	0.55	−0.01	1	9.44	0.69	2	9.00	0.37	0.30	1	F6	1, 3	60	1	216			D1
1404.....	11.51	0.84	0.34	1	10.56	0.95	5	9.81	0.60	0.47	1	G5	3, 5	34, 27, 14	3, 11, 7	220			D1
1408.....	14.40	−0.75	...	5	...	...		10.45	0.59	0.14	1	K5–K7	1	21	1	219			C1
1409.....	11.60	0.85	0.28	1	10.59	1.01	5	9.72	0.69	0.57	1	G4:, F8	1, 4	29, 45, 60	1, 5, 6	224			C3
1414.....	11.48	0.64	0.11	1	10.72	0.70	5	10.27	0.28	0.03	1	F8, G5	1, 3	29, 38, 14	1, 3, 7	225			C1
1425.....	12.00	0.91	0.34	1	11.01	1.00	4	10.15	0.41	0.15	1	G7	1	26, 33	1, 3	233			C1
1440.....	12.73	0.96	0.49	1	...	...		11.17	0.48	0.07	1	K5–K7, K0–K2	1, 4	16–20	1	244			C2
1445.....	8.15	−0.09	−0.45	1	...	...		8.33	−0.02	−0.03	1	B6, B7	1, 3, 11	280, 245	1, 8	246	36842		C1
1455.....	10.89	0.64	−0.16	4	10.08	0.76	1	9.56	0.35	0.11	1	G0	1, 2	21	1	252			D1
1484.....	12.20	1.08	...	5	10.97	1.04	1	10.27	0.49	0.11	1	K1	1	49, 44	1, 3	283			D1
1491.....	7.44	−0.06	−0.39	1	...	...		7.54	0.01	0.00	1	B8–B9	1, 3, 11	225, 220	1, 8	281	36865		C1
1505.....	12.78	0.87	0.48	1	...	...		11.06	0.57	0.09	1	K2:	1	17–20, 30	1, 3	293			C1
1507.....	10.26	0.28	0.21	1	9.96	0.30	4	9.70	0.10	0.03	1	A5, A7, A8	1, 3, 11	136, 235	1, 9	295	294265		C3
1510.....	12.40	1.25	...	5	11.09	1.31	1	10.08	0.65	0.19	2	K2	1	38, 39	1, 14	302			D1
1511.....	9.30	0.15	0.15	1	9.14	0.16	4	9.05	0.04	−0.01	1	A2	1, 3, 11	112, 180	1, 9	304	36866		D1
1518.....	13.80	0.80	...	9	11.65	1.60	1	10.28	0.72	0.24	2	K2	2	38	3	311			D1
1539.....	10.77	0.71	0.29	1	9.80	0.94	1	9.10	0.17	0.09	2	B8	1, 3	250	1	328			C3
1540.....	11.35	1.27	1.11	3	9.89	1.49	1	8.83	0.55	0.23	2	K4, K1	1, 2	15–20 (SB)	1	334			D1
1541.....	12.58	0.99	0.41	1	11.12	1.27	1	10.14	0.53	0.17	2	K1, K2, K3	1, 5, 4	11–20, 29, 15	1, 3, 14	335			D1
1552.....	13.72	1.00	−0.65	8	11.65	1.75	1	10.07	0.98	0.71	2	K7	2	15	3	340			D1
1553.....	12.40	1.36	...	5	...	...		10.09	0.77	0.47	1	K2	1	28 (SB:54)	1	339			D1
1554.....	12.30	0.88	0.43	1	...	...		10.75	0.50	0.09	1	G8, K2	1, 4	30	1	341			C4
1562.....	9.47	0.08	0.03	1	9.59	0.05	3	9.51	−0.01	−0.03	1	A0, B9	1, 3, 11	200, 250	1, 9	342	36899		C3
1581.....	12.46	0.73	0.27	1	...	...		10.76	0.34	0.09	1	F5	1	17–20 (SB:12)	1, 3	365			C1

TABLE 1—*Continued*

Parenago No.[a] (1)	V (mag) (2)	$B-V$ (mag) (3)	$U-B$ (mag) (4)	UBV Ref.[b] (5)	I_C (mag) (6)	$V-I_C$ (mag) (7)	VI Ref.[c] (8)	J (mag) (9)	$J-H$ (mag) (10)	$H-K$ (mag) (11)	JHK Ref.[d] (12)	Sp. Type (13)	Sp. Type Ref.[e] (14)	$v \sin i$[f] (km s^{-1}) (15)	$v \sin i$ Ref.[g] (16)	Brun No.[h] (17)	HD No. (18)	HR No. (19)	Group (20)
1587.....	12.60	1.30	...	5	11.11	1.61	1	9.84	0.63	0.21	2	K2	1, 2	19–20, 32	1, 14	374			D
1605.....	8.03	0.17	0.10	1	7.57	0.41	1	7.27	0.28	0.51	1	A0, B9	1, 11, 2	127, 170, 110	1, 9, 8	388	36917		D1
1608.....	12.95	1.03	0.79	1	...	...		10.91	0.63	0.10	1	K5, K4	1, 4	26	1	394			C4
1623.....	10.13	0.57	0.43	4	9.29	0.90	1	8.46	0.48	0.49	1	A3, A2	1, 2	171, 260	1, 9	405			C3
1626.....	11.24	0.68	0.14	1	10.48	0.77	5	9.89	0.31	0.07	1	A5:, G2	1, 6	94, 110	1, 7	407			C4
1634.....	8.39	−0.10	−0.48	1	...	...		8.93	−0.06	−0.04	1	B7, B9 IV	1, 3, 11	150	1	417	36918		C4
1643.....	13.30	0.63	...	5	...	...		10.95	0.54	0.18	1	K0	1	16–20, 36	1, 3	424			D1
1646.....	9.80	0.49	0.01	1	...	...		7.81	−0.03	−0.03	1	F6	1, 3	11–20	1	425	294257		C1
1654.....	8.88	0.08	−0.15	1	...	...		8.87	0.21	0.03	1	B8–B9	1, 3, 11	120	1	437	36938		C2
1657.....	11.51	0.51	−0.03	1	10.93	0.58	4	8.58	0.06	0.03	1	F2, G2	1, 4	14–20	1	438			C4
1659.....	11.62	1.21	0.77	3	10.15	1.56	1	9.03	0.64	0.30	2	K2, K3	1, 2	9–20, 7 (SB:30)	1, 14	443			D
1660.....	9.00	−0.02	−0.22	1	8.93	0.00	1	8.93	0.14	0.00	2	B8, B9	1, 11, 2	275, 375	1, 9	442	36939		D1
1664.....	7.59	−0.13	−0.55	1	...	...		8.92	0.05	0.03	1	B3, B5	1, 3, 11	180:	1	440	36936		C1
1671.....	9.65	0.26	0.11	1	...	...		9.06	0.13	0.00	1	A5–A7	1, 3, 11	175	1	454	36937		C1
1679.....	12.20	0.75	...	5	...	...		10.20	0.48	0.13	1	K2	1	18–20	1				C1
1683.....	10.93	0.46	0.38	1	10.44	0.48	3	10.05	0.12	0.05	1	A1, A0	1, 3	<50	1	464			C3
1685.....	10.19	0.15	0.14	1	9.89	0.27	1	9.39	0.26	0.25	1	B9	1, 2	201, 240/50	1, 9	466			D
1691.....	11.23	0.70	0.22	4, 5	10.42	0.81	4	9.87	0.39	0.08	1	G4	6	68	7				C
1698.....	8.87	0.06	0.01	1	...	...		8.76	0.01	0.01	1	A1	1, 3, 11	<50	1	472	36957		C1
1708.....	7.35	−0.08	−0.59	1	...	...		7.44	−0.03	−0.01	1	B3–B5, B3	1, 3, 11	<50	1	480	36958		C2
1712.....	10.47	0.57	0.25	1	9.74	0.70	3	9.15	0.23	0.13	1	B9	1, 3	75	1	479			C3
1716.....	5.71	−0.20	−0.90	1	...	...		...	...	...		B1	12, 11, 3	35, <10	12, 10	482	36959	1886	C4
1728.....	4.81	−0.25	−1.01	1	...	...		...	...	...		B0.5	12, 11, 3	25, 30	12, 10	493	36960	1887	C4
1736.....	11.11	1.27	0.74	1	9.43	1.63	1	8.26	0.54	0.26	2	F8, G2	1, 2	41, 100	1, 7	497			C3
1744.....	7.84	−0.12	−0.56	1	8.05	−0.16	1	8.12	−0.06	−0.04	1	B5, B4	1, 11, 2	75, 135, 145	1, 9, 10	502	36981		C3
1746.....	11.66	1.08	...	1	10.18	1.34	1	9.03	0.90	0.79	2	K0, K2	1, 2	36, 39	1, 3	510			D
1768.....	9.23	−0.03	−0.12	1	9.21	0.02	4	9.20	0.02	0.03	1	B9, B9.5	1, 3, 11	180	1	520	36983		C4
1772.....	8.46	0.09	−0.61	1	8.04	0.33	1	7.75	0.13	0.10	1	B2.5, 1.5p	1, 2, 11	80, 135	1, 9	530	36982		D
1785.....	12.47	1.13	...	3	11.16	1.53	1	9.77	0.88	0.65	2	K0	1	18–20, 22	1, 14	535			D
1789.....	10.53	0.53	0.01	1	9.92	0.61	4	9.51	0.24	0.04	1	F6	1, 3	81	1	540			C4
1792.....	8.88	−0.05	−0.26	2	8.92	−0.04		8.87	0.07	0.01	1	B8–A0, A0	10, 11	75	8		37001		C
1795.....	9.00	−0.01	−0.15	1	9.00	0.00	4	8.98	0.03	−0.03	1	B9	1, 11	350:	1	529	36998		C1
1798.....	9.47	0.36	−0.41	1	...	...		8.11	0.36	0.18	1	B3	1, 3, 11	50:	1	545	294264		C2
1799.....	12.64	1.14	−0.11	1	10.94	1.85	1	9.52	0.63	0.26	2	G0–G2	1	123, 10, 220	1, 3, 5	541			D1
1813.....	7.49	−0.14	−0.66	1	...	...		7.69	0.01	−0.02	1	B4, B3, B5	1, 3, 11	80	1	552	37000		C4
1828.....	12.44	1.14	0.63	3	11.05	1.43	2	9.79	0.76	0.53	1	K3	1	29	1	563			D1
1849.....	8.51	−0.09	−0.41	1	...	...		8.70	−0.03	−0.03	1	B8, B7	1, 3, 11	50:	1	581	36999		C4
1865.....	6.74	0.03	−0.87	1	6.31	0.42	1	6.09	0.28	0.16	1	O9, B0,O7	1, 2, 11	<50, 135 (SB1)	1, 9	587	37020	1893	D
1881.....	9.81	0.21	−0.10	1	...	...		9.25	0.19	0.04	1	A0–A2	1, 3	<50	1	599	294262		C2
1891.....	5.14	−0.01	−0.95	1	4.81	0.33	1	4.63	0.15	0.07	1	O7e	1, 2, 11	100:, 140, 98	1, 9, 13	598	37022	1895	D
1905.....	9.39	0.05	0.05	1	9.36	0.04	3	9.24	0.03	0.04	1	A0	1, 3, 11	177, 190	1, 9	608	37019		C3
1923.....	12.70	0.50	...	5	11.25	0.64	1	10.03	0.56	0.33	2	A5	1, 2	125, <12	1, 3	633			D
1929.....	13.30	0.48	...	5	...	...		10.05	0.76	0.42	1	K3	1	34, 50	1, 3	635			D1
1933.....	6.57	−0.14	−0.77	1	...	...		4.96	0.08	−0.01	1	B1.5–B3p	11, 12, 1, 3	125, 150	1, 10	632	37017	1890	C1
1950.....	15.00	−1.86	...	5	...	...		10.65	0.41	0.13	1	G8	1	27	1	645			C2
1953.....	9.89	0.72	0.17	1	9.05	0.83	1	8.35	0.55	0.53	1	G1, G0	1, 2	31	1	653			C3

TABLE 1—*Continued*

Parenago No.[a] (1)	V (mag) (2)	$B-V$ (mag) (3)	$U-B$ (mag) (4)	UBV Ref.[b] (5)	I_C (mag) (6)	$V-I_C$ (mag) (7)	VI Ref.[c] (8)	J (mag) (9)	$J-H$ (mag) (10)	$H-K$ (mag) (11)	JHK Ref.[d] (12)	Sp. Type (13)	Sp. Type Ref.[e] (14)	$v \sin i$[f] (km s^{-1}) (15)	$v \sin i$ Ref.[g] (16)	Brun No.[h] (17)	HD No. (18)	HR No. (19)	Group (20)
1955.....	10.91	1.09	0.60	1	9.65	1.33	1	8.75	0.59	0.21	1	G8:, G2	1, 2	109, 130	1, 7	656			C3
1956.....	9.62	0.29	−0.39	2	8.90	0.72	1	8.13	0.48	0.26	2	B3, B4	1, 2	200, 190	1, 9	655			D
1971.....	13.57	1.22	0.90	6	12.25	1.36	1	11.45	0.66	0.12	2	Late K	2	18	3	671			C3
1972.....	12.90	1.30	...	5	11.81	1.34	1	10.91	0.61	0.13	2	K3	1, 2	18–20, 12	1, 14	676			D
1973.....	12.80	1.50	...	9	11.83	1.44	1	10.53	0.79	0.53	2	G9	2	45	2	669			D
1993.....	5.06	−0.08	−0.97	1	4.97	0.10	1	4.95	0.07	0.01	1	O9–B0e	1, 2, 11	150, 145 (SB1)	1, 9/10/13	682	37041	1897	D
1996.....	11.01	0.64	0.15	1	10.21	0.78	5	9.68	0.34	0.02	1	F8, G5	1, 3	63, 51	1, 7	684			C4
2001.....	13.10	0.70	...	5	11.12	1.22	1	10.23	0.61	0.12	2	K0, K1	1, 2	7–20	1	690			D1
2006.....	12.88	1.00	0.72	6	12.49	1.34	1	11.31	0.71	0.33	4	K4	2	28	3	696			C3
2020.....	12.02	0.97	0.43	1	10.88	1.06	1	10.10	0.49	0.16	1	K2:, K0	1, 2	36, 38, 42	1, 3, 14	698			C3
2031.....	6.41	−0.11	−0.93	1	6.41	0.00	1	6.46	0.07	0.07	2	B1	1, 2, 11	50:, 30, 10	1, 9, 10	714	37042		D
2033.....	11.73	0.91	0.16	3	10.59	1.19	1	9.73	0.55	0.19	2	K1:, G5	1, 2	56, 64	1, 14	713			D
2035.....	9.80	0.20	0.13	1	9.47	0.32	4	9.48	0.02	−0.02	1	A3	1	106	1	720			C4
2036.....	9.76	0.41	0.08	1	9.24	0.52	4	8.87	0.25	0.28	1	F2	1, 3	57 (SB:15)	1	718			C4
2037.....	2.76	−0.25	−1.07	1	3.03	−0.26		3.31	...	...		O9 III	3, 11	120	13	721	37043	1899	C4
2047.....	14.00	0.90	...	9	12.37	1.75	1	11.00	0.73	0.24	2	M0	2	12	3	732			D
2048.....	13.90	1.10	...	9	12.13	1.82	1	10.85	0.70	0.15	2	K8	2	14	3	733			D1
2058.....	9.57	0.04	0.03	1	9.47	0.00	1	9.41	0.07	0.02	2	A0	1, 2	170, 200	1, 9	734			D
2065.....	9.08	−0.01	−0.20	1	...	...		9.14	−0.02	−0.03	1	B9, B8	1, 3	180	1	736	37059		C2
2069.....	12.30	1.02	...	5	10.84	1.25	1	9.95	0.64	0.06	2	K3	1	38, 44	1, 3	744			D1
2074.....	6.83	0.26	−0.69	1	6.31	0.53	1	5.84	0.19	0.09	1	B2, B1	1, 2, 11	225, 160 (SB1)	1, 9/10	747	37061		D1
2083.....	7.30	−0.13	−0.78	1	...	...		7.66	−0.02	−0.03	1	B4, B3p	1, 11	50:, <10	1, 10	761	37058		C2
2084.....	12.49	1.31	0.40	1	10.90	1.65	1	9.44	0.85	0.43	2	K3, K4	1, 2	19–20	1	757			C3
2085.....	8.21	0.02	−0.47	1	8.03	0.21	1	7.88	0.19	0.10	2	B4, B5	12, 11, 1, 2	50:, 140	1, 9	760	37062		D
2086.....	9.95	0.50	0.22	1	9.29	0.57	1	8.81	0.54	0.61	1	F5	1, 2	72 (SB:25)	1	767			D1
2100.....	11.80	0.94	...	4	10.30	1.42	1	9.32	0.67	0.17	2	K0:, G0	1, 2	72, 45, 66	1, 3, 14	773			D1
2102.....	9.36	0.04	−0.01	1	9.37	0.03	3	9.31	0.01	−0.05	1	A0	1, 3, 11	250, 200	1, 9	776	37060		C3
2118.....	9.90	0.08	0.07	1	9.80	0.08	1	9.22	0.56	0.27	1	A1, A0	1, 2	<50:, 400/50	1, 9	786			C3
2167.....	11.39	1.02	0.61	3	10.20	1.10	1	9.37	0.54	0.18	2	K0	1, 2	57	1	831			D1
2216.....	12.08	1.04	0.45	6	10.89	1.19	1	10.06	0.60	0.29	1	K2:	1	54	1	864			C3
2244.....	12.35	1.25	0.46	1	11.24	1.38	3	10.09	0.64	0.16	1	K3, K1	1, 4	51, 65	1, 5	887			C3
2247.....	10.00	0.41	0.41	1	9.60	0.70	1	8.32	1.04	1.00	1	A3	1, 2	140	1	884			D1
2252.....	11.61	0.88	0.36	1	10.52	1.00	5, 3	9.65	0.61	0.43	1	G8, G7	1, 3, 4	33, 43	1, 7	892			C3
2257.....	12.21	0.87	0.31	1	11.27	0.93	4	10.63	0.46	0.08	1	K0:	1	47, 51	1, 3	900			C2
2271.....	7.10	−0.07	−0.51	1	7.11	−0.01	1	7.20	0.02	0.06	1	B6pe	1, 2, 11	250:, 260/180	1, 9	907	37115		D1
2284.....	9.03	0.01	−0.11	1	9.07	−0.08	1	8.99	−0.02	0.01	1	B9.5, B8	1, 2, 11	180, 245	1, 9	920	37114		D1
2305.....	13.30	1.40	...	5	11.79	1.57	1	10.71	0.65	0.11	2	K6–K7	2	<12	3	935			D1
2333.....	11.70	0.88	...	5	...	...		10.10	0.40	0.09	1	K0	1	43, <12	1, 3	953			D1
2346.....	10.96	0.52	0.05	1	10.34	0.58	5, 4	9.91	0.24	−0.02	1	G0	3	88	7	961			C1
2358.....	11.00	0.61	0.07	1	10.25	0.71	5	9.74	0.28	0.06	1	G0	6	35, 58	3, 7	973			C1
2366.....	6.57	−0.17	−0.79	1	...	...		7.00	−0.07	−0.07	1	B2, B3	12, 1, 3, 11	175, 300	1, 9	980	37150	1906	D1
2368.....	13.56	1.54	1.50	1	...	...		...	...	0.15	4	K4, K6	3	24	11	982			C3
2370.....	10.60	0.56	...	5	9.77	0.71	5	9.41	0.32	0.08	1	G2	6	160	7				C
2387.....	9.22	−0.01	−0.10	1	9.24	−0.02	1	9.28	0.02	0.00	2	A0, B9	1, 2, 11	125, 190	1, 9	992	37174		D1
2404.....	11.30	0.70	0.18	1	10.48	0.76	5, 4	...	...	...		G2, G1	1, 5	29, 22	1, 7	1004			D1
2412.....	12.82	0.98	0.67	8	...	...		...	...	0.57	4	K3	9	47	11				C

TABLE 1—*Continued*

Parenago No.[a] (1)	V (mag) (2)	$B-V$ (mag) (3)	$U-B$ (mag) (4)	*UBV* Ref.[b] (5)	I_C (mag) (6)	$V-I_C$ (mag) (7)	*VI* Ref.[c] (8)	J (mag) (9)	$J-H$ (mag) (10)	$H-K$ (mag) (11)	*JHK* Ref.[d] (12)	Sp. Type (13)	Sp. Type Ref.[e] (14)	$v \sin i$[f] (km s^{-1}) (15)	$v \sin i$ Ref.[g] (16)	Brun No.[h] (17)	HD No. (18)	HR No. (19)	Group (20)
2441.....	10.76	0.70	0.15	1	9.92	0.84	5, 4	9.12	0.52	0.41	1	G2	3	18	7	1030			C1
2486.....	11.37	0.61	0.04	1	10.69	0.69	5	10.22	0.27	0.07	1	G5, G7	3, 6	120	7	1060			C3
2494.....	10.80	0.90	0.43	1	9.75	0.99	5	9.03	0.46	0.12	1	F7, G0, K0	6, 3, 4	26	7	1069			C
2602.....	6.20	−0.04	−0.73	2	...	...		...	...	...		B1.5, B2	12, 11, 7	20, 10	4, 10	1129	37356	1923	C
2660.....	11.27	0.54	0.04	7	10.65	0.62	5	10.27	0.26	−0.02	1	F6	6	175	7				C
2711.....	5.96	−0.24	−0.92	2	...	...		6.50	−0.09	−0.08	1	B1.5, IV	12, 7, 11	60, 105	4, 10		37481	1933	C
2758.....	7.61	−0.13	−0.55	2	7.77	−0.16		...	...	...		B3	10, 11	130	8		37526		C
2921.....	8.01	−0.10	−0.47	2	8.18	−0.17		...	...	...		B5–B6	10, 11	125	8		37700		C

NOTE.—Table 1 is also available in machine-readable form in the electronic edition of the *Astrophysical Journal.*

[a] Parenago 1954.

[b] *UBV* references: (1) Walker 1969; (2) Warren & Hesser 1977; (3) Penston 1973; (4) McNamara 1976; (5) McNamara et al. 1989; (6) Penston et al. 1975; (7) Rydgren & Vrba 1984; (8) Mundt & Bastien 1980; (9) Parenago 1954.

[c] *VI* references: (1) Hillenbrand 1997; (2) Penston 1973 transformed from Johnson system to Cousins system; (3) Penston et al. 1975 transformed to Cousins system; (4) McNamara 1976 transformed to Cousins system; (5) Rydgren & Vrba 1984.

[d] *JHK* references: (1) this paper, 1991 November/December OTTO observations; (2) this paper, 1992 SQIID observations; (3) this paper, 1993 NICMASS observations; (4) literature.

[e] Spectral type references: (1) this paper; (2) Hillenbrand 1997; (3) Walker 1969; (4) Walker 1983; (5) Duncan 1993; (6) Smith, Beckers, & Barden 1983; (7) Wolff, Edwards, & Preston 1982; (8) Penston et al. 1975; (9) Cohen & Kuhi 1979; (10) reference in Warren & Hesser 1977; (11) Brown et al. 1994; (12) Wolff 1990.

[f] The notation (SB:*nn*) in this column indicates a candidate spectroscopic binary with *nn* corresponding to the amplitude of the radial velocity variation among our different observations of the star. (SB1) indicates an SB1 candidate identified in previous literature; see $v \sin i$ references column.

[g] $v \sin i$ references: (1) this paper; (2) L. Hartmann 1996, private communication; (3) Duncan 1993; (4) Wolff et al. 1982; (5) Walker 1990; (6) Walker 1983; (7) Smith et al. 1983; (8) McNamara 1963 (old Slettebak system); (9) Abt, Muncaster, & Thompson 1970; (10) McNamara & Larsson 1962 (old Slettebak system); (11) Hartmann et al. 1986; (12) Abt & Hunter 1962; (13) Conti & Ebbets 1977; (14) Rhode et al. 2001.

[h] Brun 1935.

TABLE 2

DERIVED PARAMETERS

Parenago No.[a] (1)	$v \sin i$ Adopted (2)	$v \sin i$ Reference (3)	A_V (mag) (4)	$\log T_{\rm eff}$ (K) (5)	$\log L$ ($L_\odot$) (6)	R ($R_\odot$) (7)	$\log I$ (g cm^2) (8)	Convective/Radiative[b] (9)	$\log A$ (yr) (10)	M ($M_\odot$) (11)	$\Delta(H-K)$ (mag) (12)
82.....	200	5	0.10	4.037	2.15	3.40	55.43	R	6.15	3.74	...
378.....	15	5	0.08	4.025	1.84	2.51	54.98	R	6.46	2.90	−0.03
597.....	25	5	0.42	4.025	2.16	3.65	55.46	R	6.13	3.75	...
679.....	15	3	0.17	4.276	3.43	4.94	55.77	R	...	8.01	−0.04
854.....	190	5	0.20	4.130	2.56	3.54	55.49	R	6.03	4.45	−0.03
908.....	135	5	0.10	4.037	1.81	2.31	54.91	R	6.51	2.83	−0.04
1044.....	<50		0.79	4.294	3.13	3.21	55.55	R	...	6.47	−0.01
1049.....	20		1.20	3.623	1.14	7.18	55.78	C	4.52	0.71	0.70
1076.....	22	7	0.17	3.708	0.21	1.67	54.71	R	6.84	1.39	0.36
1097.....	150	5	0.14	4.053	1.95	2.50	55.05	R	6.39	3.14	0.00
1126.....	80		0.30	4.025	1.79	2.38	54.92	R	6.52	2.80	−0.04
1179.....	114		0.14	3.790	0.55	1.68	54.29	R	7.11	1.41	−0.02
1270.....	16	7	0.34	3.708	0.48	2.26	55.19	C/R	6.47	1.71	0.17
1319.....	187		1.60	3.761	0.72	2.36	54.84	R	6.80	1.72	−0.00
1322.....	70		0.49	3.736	0.66	2.45	55.14	R	6.56	1.91	0.01
1326.....	20		1.08	3.643	1.24	7.34	55.97	C	4.62	0.96	0.00
1345.....	20		0.46	3.643	0.73	4.07	55.40	C	5.57	0.84	0.04
1360.....	15	2	0.77	3.736	−0.07	1.05	53.98	R	7.46	1.00	...
1374.....	77		0.32	3.798	1.25	3.62	55.07	R	6.59	2.22	−0.01
1391.....	20		0.17	3.788	0.92	2.59	54.71	R	6.86	1.74	0.01
1393.....	20		0.42	3.748	0.58	2.11	54.82	R	6.81	1.65	−0.00
1394.....	60		0.28	3.798	1.24	3.60	55.07	R	6.59	2.21	0.25
1404.....	34	2	0.67	3.753	0.93	3.10	55.29	R	6.49	2.19	0.37
1408.....	21		0.17	3.623	0.36	1.65	55.01	C	5.78	0.68	0.02
1409.....	29		0.91	3.771	0.83	2.55	54.84	R	6.80	1.78	0.47
1414.....	29		0.20	3.766	0.60	2.00	54.55	R	6.98	1.48	−0.03
1425.....	26		0.75	3.742	0.64	2.32	55.03	R	6.66	1.82	0.04
1440.....	20		0.17	3.661	0.27	2.21	54.99	C	6.23	1.12	−0.04
1445.....	280		0.13	4.111	2.31	2.90	55.33	R	6.15	3.94	−0.02
1455.....	21		0.26	3.771	1.00	3.10	55.10	R	6.61	2.07	0.05
1484.....	49		0.84	3.708	0.79	3.22	55.56	C	6.07	1.96	−0.02
1491.....	225		0.08	4.053	2.40	4.21	55.55	R	6.05	4.10	0.01
1505.....	20		0.01	3.695	0.10	1.56	54.67	R	6.86	1.31	0.01
1507.....	136		0.45	3.907	1.16	1.99	54.40	R	6.93	1.82	−0.01
1510.....	38		1.19	3.695	0.87	3.77	55.66	C	5.83	1.72	0.03
1511.....	112		0.40	3.960	1.73	2.98	55.06	R	6.48	2.75	−0.04
1518.....	38	2	0.17	3.695	−0.10	1.24	55.29	R	7.18	1.09	0.15
1539.....	250		2.47	4.053	2.02	2.72	55.17	R	6.30	3.37	−0.05
1540.....	20		0.76	3.661	1.20	6.46	55.94	C	5.28	1.23	0.09
1541.....	20		0.38	3.695	0.48	2.40	55.21	C	6.31	1.58	0.06
1552.....	15	2	0.17	3.602	0.21	2.71	54.84	C	5.84	0.55	0.56
1553.....	28		1.53	3.695	1.01	4.41	55.81	C	5.68	1.78	0.29
1554.....	30		0.28	3.713	0.37	1.95	54.94	R	6.66	1.58	−0.00
1562.....	200		0.46	4.012	1.63	2.10	54.70	R	6.67	2.46	−0.05
1581.....	20		0.93	3.806	0.49	1.46	54.18	R	7.21	1.36	−0.00
1587.....	20		1.34	3.695	0.85	3.69	55.63	C	5.84	1.71	0.04
1605.....	127		0.29	3.933	2.16	5.54	55.70	R	6.00	3.78	0.48
1608.....	26		0.17	3.652	0.20	2.14	54.93	C	6.22	1.02	−0.01
1623.....	260		1.58	3.940	1.70	3.15	55.08	R	6.48	2.72	0.38
1626.....	94		1.76	3.917	1.30	2.23	54.55	R	6.83	1.98	−0.05
1634.....	150		0.04	4.086	2.11	2.58	55.18	R	6.27	3.51	−0.03
1643.....	20		0.17	3.719	0.06	1.33	54.35	R	7.16	1.17	0.10
1646.....	20		0.10	3.798	1.22	3.51	55.03	R	6.62	2.16	−0.07
1654.....	120		0.51	4.053	1.99	2.65	55.14	R	6.33	3.29	0.01
1657.....	20		0.17	3.778	0.57	1.82	54.42	R	7.06	1.43	−0.02
1659.....	20		0.84	3.679	1.08	5.16	55.84	C	5.47	1.46	0.16
1660.....	275		0.20	4.025	1.89	2.67	55.09	R	6.40	3.07	−0.00
1664.....	180:		0.21	4.210	2.76	3.10	55.45	R	5.98	4.93	0.05
1671.....	175		0.31	3.897	1.35	2.58	54.66	R	6.76	2.04	−0.04
1679.....	20		0.17	3.695	0.40	2.19	55.12	C	6.42	1.55	0.04
1683.....	<50		1.51	3.985	1.41	1.84	55.09	R	...	2.58	−0.04
1685.....	201		0.73	4.025	1.62	1.97	54.67	R	6.69	2.47	0.22
1691.....	68	4	0.26	3.755	0.73	2.44	54.97	R	6.71	1.82	0.01

TABLE 2—*Continued*

Parenago No.[a] (1)	$v \sin i$ Adopted (2)	$v \sin i$ Reference (3)	A_V (mag) (4)	$\log T_{\rm eff}$ (K) (5)	$\log L$ ($L_\odot$) (6)	R ($R_\odot$) (7)	$\log I$ (g cm^2) (8)	Convective/Radiative[b] (9)	$\log A$ (yr) (10)	M ($M_\odot$) (11)	$\Delta(H-K)$ (mag) (12)
1698.....	<50		0.24	3.980	1.72	2.69	54.96	R	6.53	2.68	−0.01
1708.....	<50		0.47	4.272	3.09	3.40	55.52	R	...	6.32	0.00
1712.....	75		2.03	4.025	1.89	2.67	55.09	R	6.40	3.07	0.01
1716.....	<10	6	0.24	4.377	3.88	5.24	56.14	R	...	11.30	...
1728.....	30	6	0.15	4.439	4.35	6.73	56.56	R	...	16.63	...
1736.....	41		2.10	3.761	1.51	5.83	56.03	R	5.90	3.43	0.08
1744.....	75		0.21	4.195	2.63	2.86	55.37	R	6.05	4.64	−0.02
1746.....	36		0.76	3.702	0.98	4.14	55.79	C	5.80	1.97	0.66
1768.....	180		0.17	4.025	1.64	2.01	54.69	R	6.67	2.50	0.03
1772.....	80		1.03	4.294	3.06	2.98	55.50	R	...	6.19	0.08
1785.....	20		1.14	3.719	0.78	3.04	55.50	C	6.22	2.11	0.51
1789.....	81		0.22	3.798	0.98	2.65	54.70	R	6.84	1.79	−0.01
1792.....	75	5	0.11	4.025	1.76	2.29	54.87	R	6.55	2.73	0.01
1795.....	350:		0.23	4.025	1.76	2.29	54.87	R	6.55	2.73	−0.03
1798.....	50:		1.84	4.272	2.79	2.40	55.31	R	...	5.17	0.11
1799.....	123		1.75	3.766	0.90	2.82	55.02	R	6.66	1.95	0.10
1813.....	80		0.23	4.240	2.87	3.07	55.37	R	...	5.46	0.00
1828.....	29		0.62	3.679	0.66	3.20	55.40	C	5.89	1.35	0.40
1849.....	50:		0.03	4.070	2.00	2.47	55.08	R	6.36	3.26	−0.02
1865.....	<50		1.04	4.471	4.15	4.64	56.38	R	...	14.08	0.14
1881.....	<50		0.77	3.993	1.58	2.16	54.67	R	...	2.36	−0.01
1891.....	100:		0.97	4.603	5.09	7.44	57.34	R	...	33.36	0.06
1905.....	177		0.28	3.993	1.55	2.09	54.73	R	...	2.43	0.03
1923.....	125		1.20	3.917	1.00	1.04	54.27	R	7.67	1.74	0.24
1929.....	34		0.17	3.679	0.14	1.75	54.87	C/R	6.65	1.32	0.32
1933.....	125		0.34	4.307	3.42	4.26	55.77	R	...	7.98	0.01
1950.....	27		0.17	3.736	1.31	0.55	56.04	R	5.94	3.12	0.06
1953.....	31		0.51	3.771	1.36	4.66	55.57	R	6.29	2.74	0.45
1955.....	109		1.54	3.761	1.37	4.94	55.68	R	6.22	2.83	0.06
1956.....	200		1.59	4.253	2.73	2.46	55.34	R	...	4.99	0.20
1971.....	18	2	0.02	3.623	−0.01	1.91	54.72	C	6.26	0.80	0.01
1972.....	20		1.12	3.679	0.68	3.25	55.40	C	5.87	1.35	−0.03
1973.....	45	1	2.32	3.722	1.12	4.42	55.92	C	5.92	2.65	0.31
1993.....	150		0.74	4.543	4.88	7.69	57.11	R	...	27.07	0.01
1996.....	63		0.20	3.766	0.79	2.48	54.86	R	6.79	1.77	−0.04
2001.....	20		0.17	3.708	0.16	1.56	54.59	R	6.93	1.31	0.03
2006.....	28	2	0.17	3.661	0.21	2.06	54.94	C	6.33	1.15	0.22
2020.....	36		0.64	3.719	0.62	2.52	55.25	R	6.42	1.89	0.05
2031.....	50:		0.53	4.383	3.88	5.05	56.14	R	...	11.23	0.09
2033.....	56		0.78	3.744	0.90	3.10	55.37	R	6.42	2.22	0.08
2035.....	106		0.47	3.945	1.39	2.16	54.54	R	6.82	2.06	−0.06
2036.....	57		0.14	3.826	1.26	3.22	54.88	R	6.68	2.09	0.24
2037.....	120	8	0.22	4.555	5.48	14.46	57.80	R	...	49.83	...
2047.....	12	2	0.17	3.580	0.19	2.92	54.78	C	5.74	0.41	0.03
2048.....	14	2	0.17	3.591	0.18	2.76	54.80	C	5.82	0.48	−0.04
2058.....	170		0.24	3.993	1.61	2.24	54.69	R	6.68	2.38	0.01
2065.....	180		0.19	4.037	1.74	2.13	54.81	R	6.58	2.70	−0.03
2069.....	38		0.25	3.679	0.57	2.88	55.30	C	5.99	1.34	−0.04
2074.....	225		1.68	4.383	4.17	7.06	56.39	R	...	14.23	0.03
2083.....	50:		0.19	4.200	2.85	3.59	55.36	R	...	5.38	−0.01
2084.....	20		0.88	3.661	0.65	3.43	55.36	C	5.73	1.06	0.28
2085.....	50:		0.68	4.210	2.84	3.40	55.35	R	...	5.36	0.09
2086.....	72		0.21	3.806	1.35	3.93	55.15	R	6.53	2.35	0.56
2100.....	72		1.19	3.771	1.01	3.12	55.11	R	6.60	2.09	0.05
2102.....	250		0.24	3.993	1.55	2.09	54.73	R	...	2.43	−0.06
2118.....	<50:		0.37	3.993	1.38	1.72	54.99	R	...	2.77	0.25
2167.....	57		0.80	3.719	1.07	4.27	55.90	C	5.92	2.53	0.06
2216.....	54		0.54	3.695	0.59	2.74	55.34	C	6.15	1.62	0.17
2244.....	51		1.19	3.695	0.75	3.27	55.60	C	5.96	1.67	0.00
2247.....	140		1.08	3.940	1.69	3.15	55.08	R	6.48	2.71	0.92
2252.....	33		0.58	3.736	0.73	2.66	55.26	R	6.48	2.03	0.33
2257.....	47		0.33	3.719	0.42	2.00	54.96	R	6.66	1.63	−0.01
2271.....	250:		0.19	4.111	2.90	5.71	55.39	R	...	5.55	0.07
2284.....	180		0.30	4.053	1.99	2.64	55.14	R	6.33	3.29	0.00

TABLE 2—*Continued*

Parenago No.[a] (1)	$v \sin i$ Adopted (2)	$v \sin i$ Reference (3)	A_V (mag) (4)	$\log T_{\rm eff}$ (K) (5)	$\log L$ ($L_\odot$) (6)	R ($R_\odot$) (7)	$\log I$ (g cm^2) (8)	Convective/Radiative[b] (9)	$\log A$ (yr) (10)	M ($M_\odot$) (11)	$\Delta(H-K)$ (mag) (12)
2305.....	< 12	2	0.40	3.612	0.43	3.34	55.05	C	5.67	0.58	−0.04
2333.....	43		0.36	3.719	0.78	3.03	55.50	C	6.23	2.10	−0.01
2346.....	88	4	0.17	3.771	0.79	2.43	54.77	R	6.84	1.71	−0.08
2358.....	35	2	0.17	3.771	0.78	2.39	54.75	R	6.85	1.69	0.00
2366.....	175		0.25	4.309	3.54	4.80	55.86	R	...	8.66	−0.04
2368.....	24	7	1.32	3.643	0.45	2.96	55.12	C	5.82	0.85	−0.04
2370.....	160	4	0.17	3.761	0.94	3.03	55.19	R	6.55	2.12	0.02
2387.....	125		0.17	4.010	1.75	2.44	54.90	R	6.53	2.73	−0.00
2404.....	29		0.33	3.761	0.87	2.79	55.08	R	6.63	1.98	...
2412.....	47	7	0.12	3.679	0.17	1.81	54.93	C/R	6.60	1.33	0.47
2441.....	18	4	0.33	3.761	0.94	3.03	55.20	R	6.55	2.12	0.34
2486.....	120	4	0.17	3.745	0.65	2.33	55.01	R	6.68	1.82	0.00
2494.....	26	4	0.85	3.753	1.15	3.96	55.55	R	6.31	2.55	0.01
2602.....	20	3	0.68	4.332	3.76	5.62	56.04	R	...	10.29	...
2660.....	175	4	0.22	3.795	0.68	1.91	54.39	R	7.05	1.48	−0.07
2711.....	60	3	0.09	4.352	3.67	4.58	55.96	R	...	9.55	−0.04
2758.....	130	5	0.32	4.272	2.92	2.81	55.41	R	...	5.65	...
2921.....	125	5	0.13	4.125	2.39	2.99	55.36	R	6.12	4.10	...

NOTE.—Table 2 is also available in machine-readable form in the electronic edition of the *Astrophysical Journal.*

[a] Parenago 1954.

[b] C and R indicate whether star is on convective vs. radiative track in the H-R diagram.

REFERENCES.—This paper unless otherwise indicated as (1) L. Hartmann 1986, private communication; (2) Duncan 1993; (3) Wolff, Edwards, & Preston 1982; (4) Smith et al. 1983; (5) McNamara 1963; (6) McNamara & Larsson 1962; (7) L. Hartmann 1996, private communication; (8) Conti & Ebbets 1977.

photometer mounted on the KPNO 50 inch telescope. The data were taken using a standard beam-switching pattern (source/sky/sky/source) through a 15″ beam with a 30″ throw. Calibration was performed with the standards of Elias et al. (1982), thus placing the data on the CIT photometric system within color terms of order 5% (Kenyon 1988). Some measurements were adopted from the SQIID and NICMASS imaging photometry described by Hillenbrand et al. (1998). The infrared data are summarized in Table 1.

Values of $\Delta(H-K)$ are listed in Table 2; stars with $\Delta(H-K) > 0.1$ mag are considered disk candidates. Our results show that only 20% of the stars in our sample show excesses this large and only 14 of these stars lie on convective tracks where we might expect the stellar magnetic fields required for disk locking to be present. Given the small number of stars with excesses, it was impossible to effect a statistically meaningful comparison of $N(v \sin i)$ between stars that show, and those that lack, inner accretion disk signatures, given the broad intrinsic range of rotational velocities characterizing stars in this mass range. While we have made no further use of the IR data, we provide the measurements here for completeness.

2.4. *Optical Photometry*

The optical measurements in Table 1 were culled from the literature (Walker 1969; Warren & Hesser 1977; Penston 1973; McNamara 1976; Rydgren & Vrba 1984; Penston, Hunter, & O'Neill 1975; McNamara et al. 1989). Measurements of I magnitudes and $V-I$ colors are available for a subset of the sample, largely from the study by Hillenbrand (1997) but also from the above references, which have been converted from Johnson to Cousins system photometry.

2.5. *Effective Temperatures and Stellar Luminosities*

Effective temperatures are listed in Table 2 and were derived from the spectral types listed in Table 1 and the effective temperature scale of Chlebowski & Garmany (1991) for O-type stars and Humphreys & McElroy (1984) for B0–B3 stars. For stars with later spectral types, we used the temperature scales of Cohen & Kuhi (1979) and Bessell (1991). We estimate typical uncertainties in $\log T_{\rm eff}$ to be 0.05 for stars A5 and earlier, 0.03 for stars A5–G5, and 0.02 for stars G5–K5.

For low-mass PMS stars of type K and later, veiling emission at the V band can be significant, and it is preferable to use I- or J-band measurements to derive luminosities. For

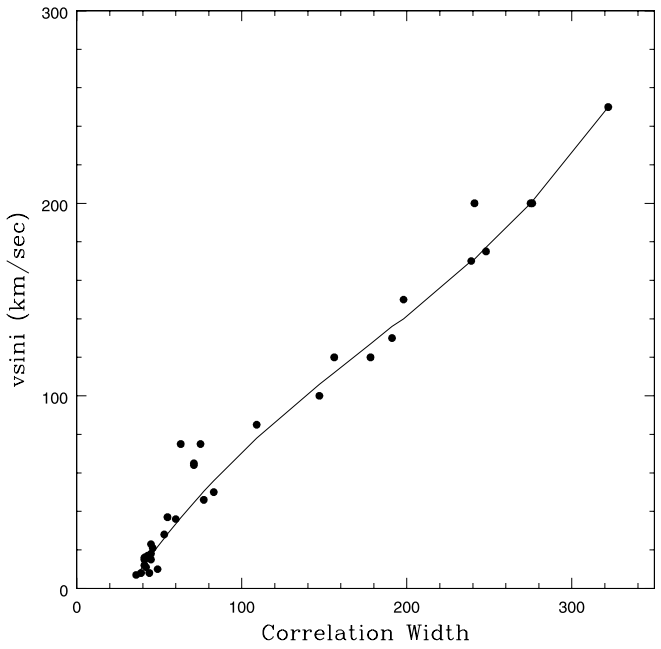

FIG. 1.—FWHM of cross-correlation peak vs. observed values of $v \sin i$ for standard stars used to establish functional relationship. The line shows the polynomial fit to the data.

stars in the current sample, which have much earlier spectral types, veiling contributions at the V band are negligible. Therefore, in order to derive stellar luminosities, we first derive extinction estimates, A_V (Table 2), on the basis of spectral types and the observed $B-V$ colors compared with intrinsic stellar colors (Johnson 1966). Next, we derive apparent bolometric luminosities from reddening-corrected V magnitudes and bolometric corrections tabulated by Code et al. (1976), Massey, Parker, & Garmany (1989), and Bessell (1991). The bolometric corrections for the PMS stars in our sample are all less than 0.25 mag. We estimate that the standard errors in apparent bolometric magnitude are ± 0.15 mag.

Conversion of apparent bolometric magnitude to luminosity requires a distance modulus. Studies of the Orion association suggest that members of the star-forming complex may span distances ranging from $\sim$350 to 500 pc (Brown et al. 1994). Most of the stars composing our sample fall in two well-studied regions of the association: Orion Id, a region of size $\sim$2 pc centered on the Trapezium cluster, and Orion Ic, also centered on the Trapezium but extending 10 pc in projection from θ^1C. The best distance estimates for these subregions of the association are 480 pc for Orion Id (based on water maser proper-motion and radial velocity measurements; Genzel & Stutzki 1989) and 400 pc for Orion Ic (based on careful photometric study of ZAMS B stars; Warren & Hesser 1978). Assignment of a sample star to the Orion Ic or Id subregions (see col. [20] of Table 1) is based on its *projected* location on the plane of the sky in relationship to the Ic/Id boundaries delineated in the map published by Warren & Hesser (1977). This procedure means that a modest fraction of the stars assigned as Id could actually be Ic stars seen in projection on Id.

The values of $\log L$ listed in Table 2 have estimated uncertainties of ± 0.2 dex, resulting from uncertainties in the assigned distances, temperatures, and bolometric corrections. Given values of $\log L$ and $T_{\rm eff}$, we can derive the stellar radius, which is also given in Table 2.

2.6. *Masses, Ages, and Moments of Inertia*

The luminosities and effective temperatures listed in Table 2 enable the determination of masses, ages, and stellar moments of inertia via comparison with PMS evolutionary tracks. The tracks published by Swenson et al. (1994, hereafter SFRI) are used here because (1) they span the range of masses encompassed by our sample; (2) they include not only luminosity (L) and effective temperature ($T_{\rm eff}$) but also moments of inertia (I) as a function of age; and (3) they provide the best matches to open cluster loci (L. A. Hillenbrand 2004, in preparation). The derived values of mass (M), age ($\log A$), and moment of inertia ($\log I$) are listed in Table 2. On the basis of the values of L and $T_{\rm eff}$ and the evolutionary tracks, we also specify whether the star is on the convective (C) or radiative (R) portion of its evolutionary track or at the convective/radiative transition (C/R) in column (9).

Uncertainty in transforming $L_{\rm bol}$ and $T_{\rm eff}$ to mass and age for PMS stars is dominated by systematic effects between different sets of PMS evolutionary tracks, rather than by random errors associated with the luminosity and $T_{\rm eff}$ derivations. Unfortunately, there are few model-independent determinations of masses for stars above the ZAMS (e.g., Mathieu et al. 2000). We also note that the SFRI tracks do not take into account the effects of accretion during early PMS phases. Accretion can dramatically alter both the evolutionary path of PMS stars and the radius at which a star of a given final mass joins *conventional* PMS tracks. In particular, accreting PMS stars follow paths (birth lines) roughly parallel to the ZAMS, at distances above the ZAMS that depend on the mass accretion rate (e.g., Palla & Stahler 1992). For example, a young star can in principle reach the same point in the H-R diagram by following (1) a high accretion rate birth line at large radius and then contracting toward smaller radii along a *conventional* convective track or (2) a low accretion rate birth line that deposits it directly at relatively low radius. Because of the different possible approaches to the main sequence, the ages assigned to nonaccreting PMS stars and both the ages and masses assigned to accreting PMS stars from comparisons of observed luminosities and effective temperatures with conventional tracks should be regarded with caution.

3. THE RELATIONSHIP BETWEEN SPECIFIC ANGULAR MOMENTUM AND MASS

3.1. *Overview*

Our measurements of the Orion stars provide for the first time a snapshot of the distribution of angular momenta among a sample of very young (1–10 Myr) stars, presumably formed under similar initial conditions, spanning a mass range from less than 1 $M_\odot$ to slightly more than 10 $M_\odot$, and including a sample of fully convective stars with masses in the range 1–2 $M_\odot$. The mean and median masses within our sample are 2.9 and 2.1 $M_\odot$. These data allow us to assess systematic trends in stellar angular momenta with mass and time.

In this section we first plot our entire sample in the H-R diagram and describe the systematic trends between surface rotational velocity and mass. We then separate the data into two groups: (1) those stars that are still on their convective tracks and provide us with the best estimates of the initial values of specific angular momentum (J/M) and (2) more evolved stars that are on PMS radiative tracks or on the main sequence. We then compare the observationally derived initial values of J/M with those of stars at later phases of their evolution and identify the processes that most plausibly control the evolution of angular momentum.

3.2. *The Data*

Figure 2 summarizes the rotation data for the Orion stars observed as part of this survey. We see that the distribution of stars in the H-R diagram is what we expect for objects that range in age from less than 1 Myr to nearly 10 Myr. The more massive stars ($M > 4\ M_\odot$) are already on the main sequence. Intermediate-mass stars ($2\ M_\odot < M < 4\ M_\odot$) occupy a variety of positions along the radiative tracks; theory (e.g., Palla & Stahler 1992; Behrend & Maeder 2001) predicts that depending on the accretion rate, stars with $M > 2$–$4\ M_\odot$ will already be radiatively stable when they reach their birth lines and begin quasi-static contraction. Most of the Orion stars with $M < 2\ M_\odot$ are still on their convective tracks.

3.3. *Specific Angular Momentum as a Function of Mass*

The specific angular momentum of a star is given by the relationship

$$\frac{J}{M} = \frac{I\omega}{M}, \tag{1}$$

where J is the total angular momentum, M is the mass of the star, I is the moment of inertia, and ω is the angular velocity.

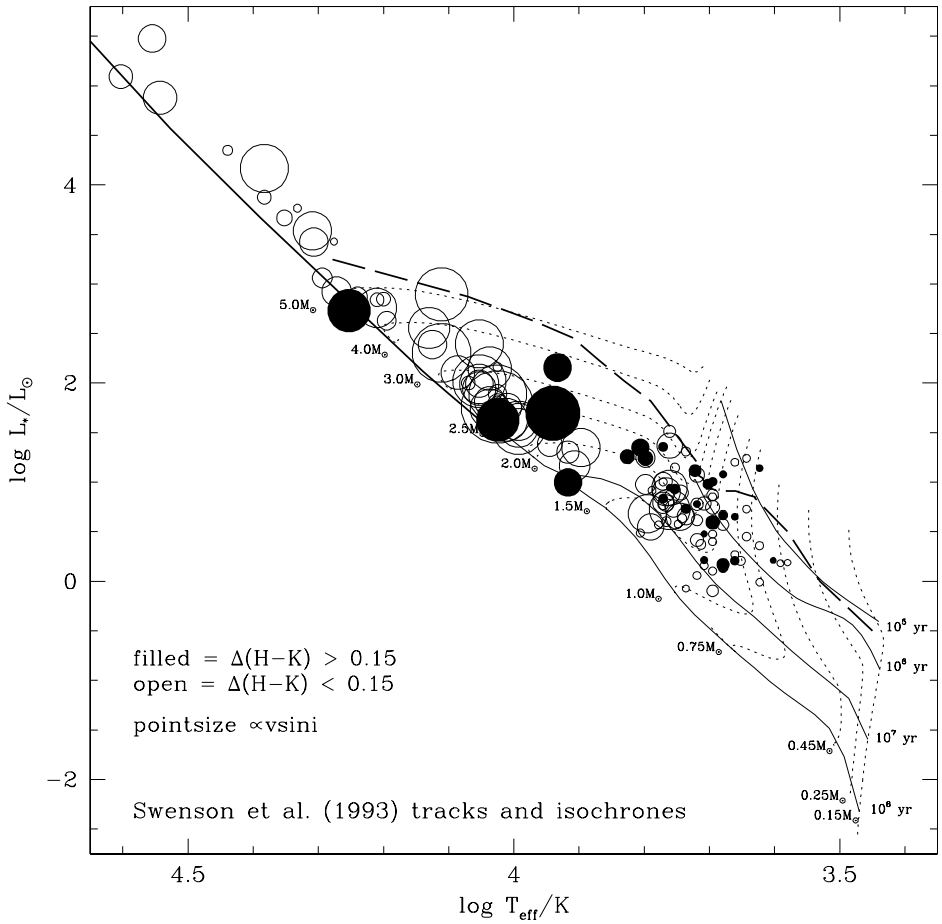

FIG. 2.—H-R diagram for stars in the current sample. Circle size is proportional to the observed rotation ($v \sin i$). Filled circles represent stars with infrared excesses, which are diagnostic of inner accretion disks. The light dashed lines are evolutionary tracks from SFRI. The heavy line with long dashes shows the location of the PS birth line for an accretion rate of $10^{-5}\ M_\odot\ \mathrm{yr}^{-1}$ (Palla & Stahler 1993). The solid lines are the isochrones of SFRI from 10^5 to 10^8 yr (uncorrected for the birth line).

What we measure is $v \sin i$, so we can calculate only $J \sin i$. For a large sample of stars and a random distribution of axes, $J = (4/\pi)J \sin i$ (for derivation see Chandrasekhar & Munch 1950).

Figure 3*a* shows the plot of projected specific angular momentum as a function of mass for stars that are still on their convective tracks along with stars hotter than $\log T_{\rm eff} = 4.0$, which are already on the ZAMS. To extend the data to lower masses, we have also plotted $J \sin i$ values derived from the $v \sin i$ study of low-mass Orion Nebula cluster (ONC) stars on convective tracks by Rhode et al. (2001). We have used the SFRI models to derive values of I for each of their stars.

PMS stars on convective tracks rotate well below the critical velocity at which centrifugal and gravitational forces balance—the so-called breakup velocity. To show this, we have plotted in Figure 3*a* the specific angular momentum that corresponds to rotation at the critical velocity for stars on the Palla & Stahler (1993) birth line (PS birth line). The PS birth line intersects SFRI convective tracks for masses below 3 $M_\odot$ and intersects radiative tracks for masses above 3.5 $M_\odot$. The discontinuity in the breakup velocity curve for stars on the birth line with masses between 3 and 3.5 $M_\odot$ comes about because I, the moment of inertia, becomes significantly smaller once stars join their radiative tracks, at which point they become much more centrally condensed.

Figure 3*a* shows that there is a fairly smooth and slowly varying upper bound to $J \sin i/M$ defined by fully convective stars with masses less than 2.5 $M_\odot$; since these stars are expected to rotate as solid bodies, their surface rotation rates should reflect true values of J. This upper bound then merges continuously with the upper bound determined by higher mass stars that have already reached the ZAMS. The five stars that lie well above the upper bound shown in Figure 3*a* also lie at the tops of their convective tracks and are more luminous than most of the other Orion stars in our sample. It may be that, because of depth effects in the cluster, the luminosities and hence the radii and angular momenta of these five stars are overestimated, or it may be that they are indeed very young and rotating more rapidly than the remaining Orion stars (see the discussion in § 6).

There is about an order of magnitude scatter below the upper bound shown in Figure 3*a*. The scatter is too large to be accounted for by projection effects alone because there is only a 14% chance of observing a rotation rate that is less than 50% of the true equatorial velocity. Physical factors that may also contribute to the observed scatter are discussed in § 4.

Kraft (1970) looked at a sample of mature main-sequence stars and found that a power law describes the relationship between $\langle J/M \rangle$ and M for *main-sequence stars* with $M > 2\ M_\odot$ (but not those with smaller masses). Specifically, he found that $\langle J/M \rangle$ varies as $M^{0.57}$, and this relationship is referred to as the "Kraft law." Kawaler (1987) found the same basic relationship but with $\langle J/M \rangle$ proportional to $M^{1.02}$. Kraft

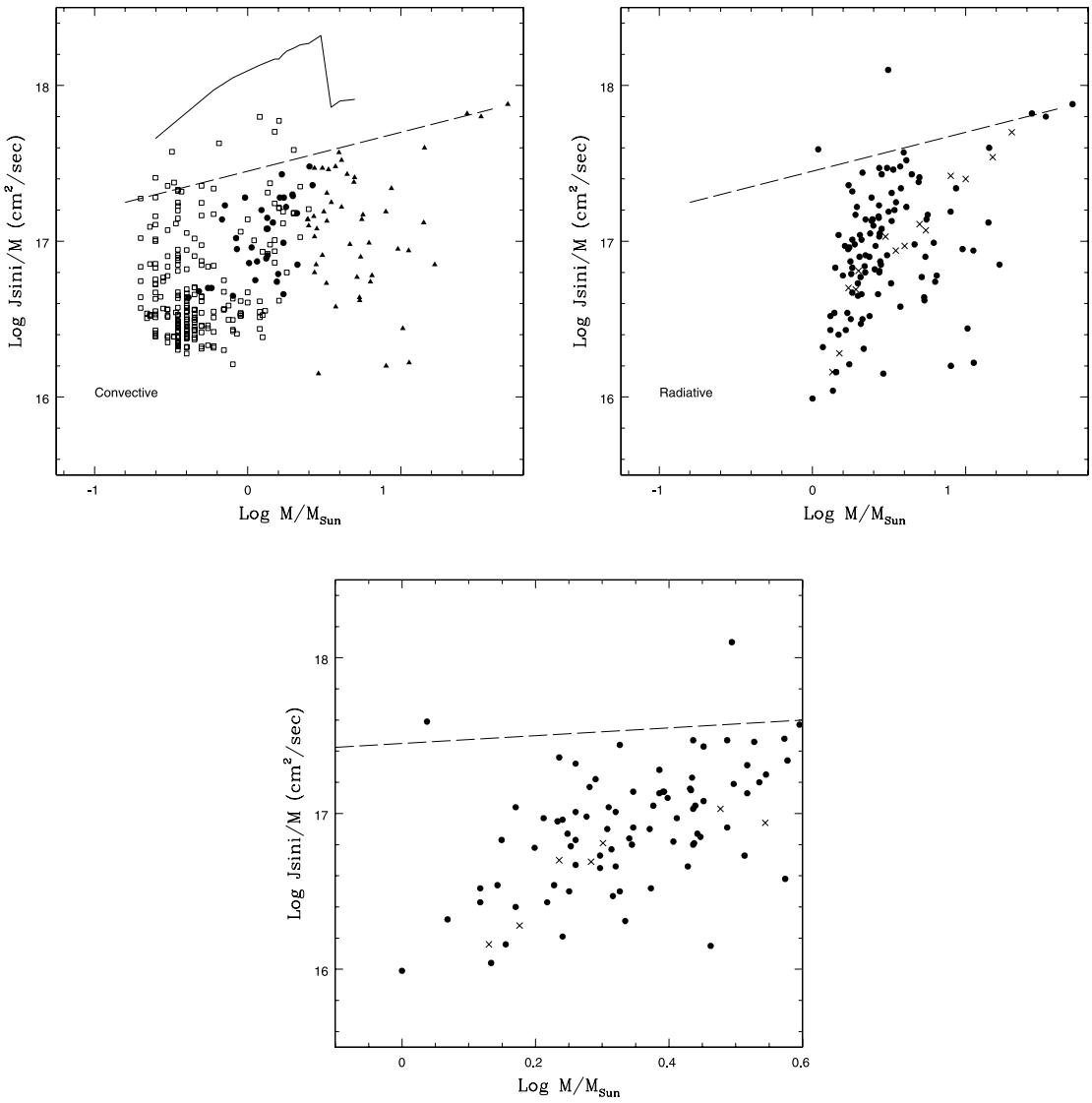

FIG. 3.—(*a*) Values of specific angular momentum ($J \sin i/M$) as a function of mass for stars on PMS convective tracks. Circles represent Orion stars in the current sample that are on convective tracks; squares are similarly analyzed data from the study by Rhode et al. (2001) of primarily lower mass stars in the ONC; triangles represent Orion stars with $T_{\rm eff} > 10,000$ K, which are already on the main sequence. The solid line shows the specific angular momentum corresponding to rotation at the breakup velocity along the PS birth line. The break in this curve occurs in the mass range where the birth line changes from intersecting convective tracks ($M < 3\ M_{\odot}$) to intersecting radiative tracks ($M > 3.5\ M_{\odot}$). The dashed line is a fit by eye to the upper bound of the data and has slope 0.25. (*b*) Specific angular momentum of stars that have completed the convective phase of evolution. Filled circles represent stars in Orion that are either on radiative PMS tracks or on the ZAMS. Stars with $T_{\rm eff} > 10,000$ K and the dashed line are repeated from (*a*). Crosses represent the average values of $J \sin i/M$ for field stars taken from data in the literature (see text for references). (*c*) Enlargement of the region of (*b*) for masses in the range 1–3 $M_{\odot}$. Note the downturn in $J \sin i/M$ for both the Orion and field stars for masses less than about 2 $M_{\odot}$. This downturn is not seen in convective PMS stars in (*a*).

and Kawaler both found a marked steepening in the slope below about 2 $M_{\odot}$. In Figure 3*a* we see that the power-law relationship for PMS stars on convective tracks extends to masses at least as low as 0.1 $M_{\odot}$. The slope of the relationship for PMS convective stars does *not* change at 2 $M_{\odot}$, and the value of the slope is about 0.25, somewhat shallower than found by Kraft for main-sequence stars with $M > 2\ M_{\odot}$.

Figure 3*b* shows the same plot but this time for Orion stars that are either on their PMS *radiative* tracks or on the ZAMS. Orion is not old enough to contain stars with $M < 1\ M_{\odot}$ on radiative tracks. (The data for ZAMS stars with $\log T_{\rm eff} > 4.0$ are repeated from Fig. 3*a*.) We have 42 stars in Orion with $M > 3\ M_{\odot}$, which is a small number to define the average behavior over a large mass range, and these stars may not be fully representative, including as they do at least one He-strong magnetic star (HD 37017) and several other peculiar and emission-line stars. Therefore, we also show in Figure 3*b* the average values of $\langle J \sin i/M \rangle$ for a larger sample of main-sequence field stars as a function of mass. We obtained these values by using $\langle v \sin i \rangle$ data from Abt, Levato, & Grosso (2002), Abt & Morrell (1995), and Wolff & Simon (1997); moments of inertia from the SFRI models for ZAMS stars (we extrapolated these models to obtain I for masses greater than 5 $M_{\odot}$); temperatures derived from spectral types for the B- and early A-type stars (Cox 2000, p. 388); and masses as a function of temperature from the models of SFRI and Maeder & Meynet (1988). For the F-type stars, we adopted the calibrations used by Wolff and Simon.

From Figure 3*b* we see that the PMS stars on radiative tracks in Orion scatter fairly reasonably around the mean values for field stars (see also Fig. 3*c*). There is also a strong similarity in the overall behavior of the Orion PMS stars on radiative tracks and the main-sequence field stars. Both groups show a relatively slow decline in specific angular momentum over a mass range of a factor of 10 (from 30 to 3 $M_\odot$). From 3 $M_\odot$ to about 1 $M_\odot$ (Orion) or 1.4 $M_\odot$ (field stars), the specific angular momentum declines by an additional order of magnitude for both groups. Below about 1.4 $M_\odot$, but not at higher masses, stars are believed to lose angular momentum through magnetic winds during the first several hundred million years after they reach the ZAMS (e.g., Kraft 1970; Wolff and Simon 1997), so the slope for $M < 1.4\ M_\odot$ depends on the age of the main-sequence stars in the sample. Comparison of PMS stars with main-sequence field stars at $M < 1.4\ M_\odot$ is therefore not relevant.

These trends in angular momentum as a function of mass are well known for main-sequence stars. What is new here is the discovery that the overall trend of steep decline in average values of angular momentum for masses between 1 and 2 $M_\odot$ *is already present in PMS stars that are on their radiative tracks and that are typically no more than a few million years old*. As Wolff & Simon (1997) suspected from their study of main-sequence stars, an overall decline in angular momentum along the main sequence from 2 $M_\odot$ to at least 1 $M_\odot$ is apparently imposed during the PMS phase of evolution, and this pattern changes little during subsequent main-sequence evolution. This point is illustrated more clearly in Figure 3*c*, which magnifies the critical region of Figure 3*b*. Here we see that with decreasing mass below 2 $M_\odot$ both the Orion PMS stars on radiative tracks and the field stars fall progressively farther away from the power-law relationship that described the upper bound for PMS convective stars (Fig. 3*a*).

In the sections that follow, we compare the data in Figure 3*a* on initial angular momenta with a very simple model of star formation to illustrate the feasibility of using angular momentum as an additional constraint on such models. We then examine what physical processes might account for the changes in angular momentum as stars evolve from their convective tracks, as seen in Figure 3*a*, onto their radiative tracks, as seen in Figure 3*b*.

4. INITIAL ANGULAR MOMENTUM: A CONSTRAINT ON MODELS OF STAR FORMATION

The continuity of the upper bound for J/M in Figure 3*a* suggests that the origin of stellar angular momenta is likely similar for stars with masses spanning at least 2 orders of magnitude, from 0.1 to 10 $M_\odot$. To illustrate the feasibility of relating this observation to theories of star formation, we consider the implications of one very simple model, which attributes the observed slow rotation of PMS stars to a magnetic field that is rooted in the central star and intercepts the disk (e.g., Königl 1991). The net consequence of this star-disk interaction is that stellar angular velocity is locked to the Keplerian angular velocity at a corotation radius until the accretion phase ends and the star is deposited on the birth line. According to Königl, the angular velocity of a star locked to its disk is given by

$$\varpi = \epsilon \left(\frac{GM}{R_{\rm in}^3} \right)^{1/2}, \tag{2}$$

where $\epsilon < 1$ is the ratio between the stellar angular velocity and the Keplerian velocity at $R_{\rm in}$, i.e., at the radius where the disk is disrupted. This radius in turn is given by

$$R_{\rm in} = \beta \mu^{4/7} (2GM)^{-1/7} \dot{M}^{-2/7}, \tag{3}$$

where β is a parameter less than or equal to 1 (with $\beta = 1$ corresponding to the classical Alfvén radius for spherical accretion), μ is the stellar dipole moment, and $\dot{M}$ is the mass accretion rate. Using these equations plus the relationship that the surface magnetic field $B = \mu/R^3$, we then find that

$$\frac{J}{M} = \frac{I\varpi}{M} = \frac{I\epsilon (GM)^{5/7} (2)^{3/14} \dot{M}^{3/7}}{M\beta^{3/2} B^{6/7} R^{18/7}}. \tag{4}$$

In order to evaluate this expression, we must make a number of assumptions. If we set $\epsilon = \beta = 1$, then we will obtain an upper limit for J/M. We used the SFRI models to obtain values of I and R at the birth line. Since these models do not extend above 5 $M_\odot$, we have not calculated J/M beyond this mass limit. We have adopted $B = 2500$ G, which is typical of the limited measurements to date for T Tauri stars (e.g., Guenther et al. 1999; Johns-Krull, Valenti, & Koresko 1999). The number of observational constraints on this assumption is minimal (magnetic fields have been measured in fewer than 10 T Tauri stars). However, the observed constancy of magnetic field surrogates, such as $L_{\rm X}/L_{\rm bol}$, over a wide range of PMS star rotation rates (Feigelson et al. 2003) suggests that this assumption may be acceptable as a first guess.

We have carried out the calculation for two birth lines. The first is the PS birth line for $\dot{M} = 10^{-5}\ M_\odot\ {\rm yr}^{-1}$ (Palla & Stahler 1993). The second was calculated by Behrend & Maeder (2001), to which we will refer as the BM birth line, and is parameterized in terms of luminosity. The BM birth line yields results very close to a birth line (Norberg & Maeder 2000) calculated for an accretion rate given by $\dot{M} = 10^{-5}(1, M^{1.5})$, whichever is larger.

The comparison of the predicted values of J/M with the observed $J \sin i/M$ values of PMS stars on their convective tracks (i.e., the youngest stars in our sample, which are shown in Fig. 3*a*) is illustrated in Figure 4. It is remarkable that the very simple assumptions made here yield both a zero point and a slope that are reasonably close to what is observed. Within the framework of the disk-locking model, star-to-star differences in magnetic field strength, accretion rates, or the length of time that disk locking is effective, in addition to projection effects, may all contribute to the broad scattering of stars below the upper bound.

Virtually all details of putative disk-locking mechanisms are currently under debate, from the linkage of stellar magnetic fields to the disk to the basic mechanism for angular momentum loss, i.e., through the disk or through a wind (Shu et al.1994). For example, within the past year, Johns-Krull & Gafford (2002) have extended the Shu et al. model to include complex, nondipole field topologies, which they argue provide a more realistic representation of currently available observations. While this model has many attractive features, it and other more complex formulations introduce additional parameters, which must be derived empirically and which have not yet been well established. Nevertheless, the approximate coincidence between the observed J/M versus M

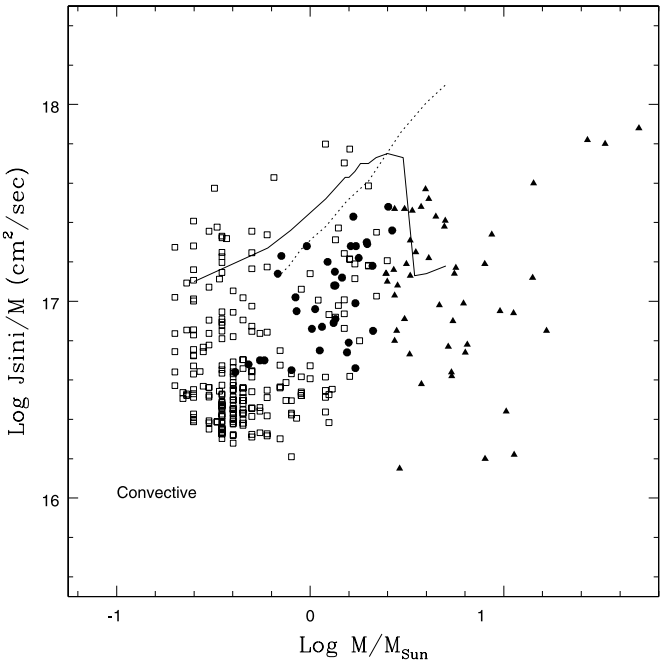

FIG. 4.—Predicted values of J/M along the PS birth line (*solid line*) and the BM birth line (*dotted line*), assuming that the rotation of protostars is locked to their disks at least until they are released on the birth line. The data are the same as shown in Fig. 3*a*. The break at 3 $M_\odot$ in the curve for the PS birth line occurs where the birth line changes from intersecting convective tracks to intersecting radiative tracks. This transition takes place at $M > 5\ M_\odot$ for the higher accretion rates used to calculate the BM birth line.

relationship and the predictions of this very simple model should serve as a challenge to theorists to develop a truly predictive theory of angular momentum loss during the disk accretion phase.

5. FROM THE BIRTH LINE TO THE MAIN SEQUENCE

Next we turn to the question of what happens to angular momentum as intermediate-mass PMS stars evolve from convective to radiative tracks and finally onto the main sequence. The observable diagnostic is the surface rotational velocity, which in turn depends on the initial angular momentum plus any modifications caused either by the transport of angular momentum from the stellar interior or by external forces, including mass accretion and mass loss, particularly when the stellar magnetic field is strong. In the sections that follow, we first look for evidence relating to the question of whether or not external forces are likely to alter the initial stellar angular momentum of PMS stars. We then look at the issue of how structural changes affect the observed rotational velocities. Informed by this discussion, we predict ZAMS rotational velocities for the stars in our sample and compare these predictions with observations of stellar rotation among young field stars. This provides the basis for evaluating how well trends of rotation with mass along the main sequence can be predicted from patterns already present during early PMS evolution.

5.1. *External Forces: Disk Regulation on Convective Tracks*

If no external forces were acting, PMS stars should spin up as they contract toward the ZAMS because of structural changes: a decrease in radius and an increase in central concentration. Some stars may also lose angular momentum as they evolve down their convective tracks, possibly as a consequence of magnetic torques that transfer angular momentum away from the star to a surrounding disk. Our current sample does not allow us to search for systematic changes in J/M as stars with $M > 1\ M_\odot$ evolve down their convective tracks. The reasons are twofold: (1) our sample spans a relatively large mass range but has relatively few stars at any given mass that are still on their convective tracks, and we cannot subdivide the sample according to mass and position along the convective track and retain sufficient numbers to average out star-to-star fluctuations in v and $\sin i$; and (2) these relatively massive stars evolve down only a truncated portion of the convective track (Palla & Stahler 1992) and do not, therefore, change in radius by more than about a factor of 2; as a result, any systematic changes in $v \sin i$ will be small relative to the dispersion in v at a given position along the convective tracks. As we discuss in § 6, however, the systematic differences in J/M for stars on convective and radiative tracks do appear to require some loss of angular momentum as stars with $M < 2\ M_\odot$ evolve down their convective tracks.

5.2. *External Forces: Mass Loss*

Stellar winds loaded onto open magnetic field lines can exert a spin-down torque on stars. This mechanism has, however, been shown to be ineffective for fully convective stars because the PMS timescale for spin-down exceeds the evolutionary timescale by a few orders of magnitude (e.g., MacGregor & Charbonneau 1994). Fully convective stars are assumed to rotate as solid bodies, and the wind must slow down the entire star—which fact precludes significant spin-down during the relatively short PMS convective phase.

Mass loss is also unlikely to have a significant effect on the angular momentum of most stars with $M > 1\ M_\odot$ that are evolving along their radiative tracks. The majority of these stars are hotter than $\log T_{\rm eff} = 3.8$, do not have surface convective zones, and are not expected to have dynamo-generated magnetic fields. This expectation is borne out by observations of X-rays from PMS stars in Orion. X-ray emission can serve as a proxy indicator of magnetic fields. Observations show that the ratio of X-ray to bolometric luminosity drops by more than 2 orders of magnitude when PMS stars become fully radiative (Flaccomio et al. 2003), and X-ray observations of PMS Orion stars show that strong X-ray emission is present only in stars cooler than $\log T_{\rm eff} = 3.8$ (Gagne, Caillault, & Stauffer 1995; Feigelson et al. 2002). About 10% of the stars with spectral types around A0 and earlier, including the He-rich star HD 37017 in our sample, do have large (several thousand gauss) magnetic fields that are thought to be fossil rather than dynamo-generated fields, and it is not known how these large fields might affect either the initial angular momentum or the subsequent evolution of angular momentum. However, the number of such peculiar stars is small enough that even if some are included in the sample, they should not affect the overall trends shown in Figure 3. For the purposes of this paper, we will assume that very few stars hotter than $\log T_{\rm eff} = 3.8$ have strong surface fields, and they are therefore unlikely to experience strong braking torques caused by stellar winds.

5.3. *Internal Effects: Changes in the Moment of Inertia*

Even if external forces play no role, we do expect that changes in the moment of inertia will affect stellar rotation. As a star contracts and moves down its convective track and then

along a radiative track, its radius decreases and its central concentration increases. Both effects should increase the rotation rate. Whether or not increasing central concentration has an effect on the rotation rate at the *stellar surface* depends on the timescale for the transport of angular momentum from the stellar core to the surface of the star. Since the theory of this process has substantial uncertainties, we will bracket the true situation by considering two extreme cases for how angular momentum might be conserved: (1) conservation of angular momentum in shells and (2) solid-body rotation.

If angular momentum cannot be efficiently transported across adjacent spherical shells or from the radiative core to the convective envelope, then at any given time t the rotational velocity v is given by

$$v(t) = v_0 \frac{R_0}{R(t)}, \tag{5}$$

where R is the radius of the star and v_0 and R_0 refer to initial values. If, on the other hand, angular momentum is transported efficiently throughout the star and the star effectively rotates as a solid body, then

$$v(t) = v_0 \frac{I_0}{R_0} \frac{R(t)}{I(t)}, \tag{6}$$

where I is the stellar moment of inertia.

Figure 5 compares these two cases for four different stellar masses, on the basis of the models by SFRI. We have assumed arbitrarily a rotation of 10 km s^{-1} for the starting point on the tracks. Three different regions should be distinguished in this figure: (1) the fully convective phase, which we will take to be the evolution that takes place at nearly constant $T_{\rm eff}$ to the point of minimum luminosity; (2) the transition from the convective to the radiative tracks, which we will take to be the portion of the evolutionary tracks from minimum luminosity to $\log T_{\rm eff} = 3.8$, at which temperature all of the stars in our sample are on radiative tracks; and (3) the remainder of the radiative track to the main sequence.

As Figure 5 shows, during the fully convective phase, the two extreme cases for angular momentum conservation predict essentially the same evolution of surface rotation rate. As stars evolve down their convective tracks, contraction is nearly homologous, and changes in I directly correspond to changes in R^2. Along the radiative tracks, the two extreme

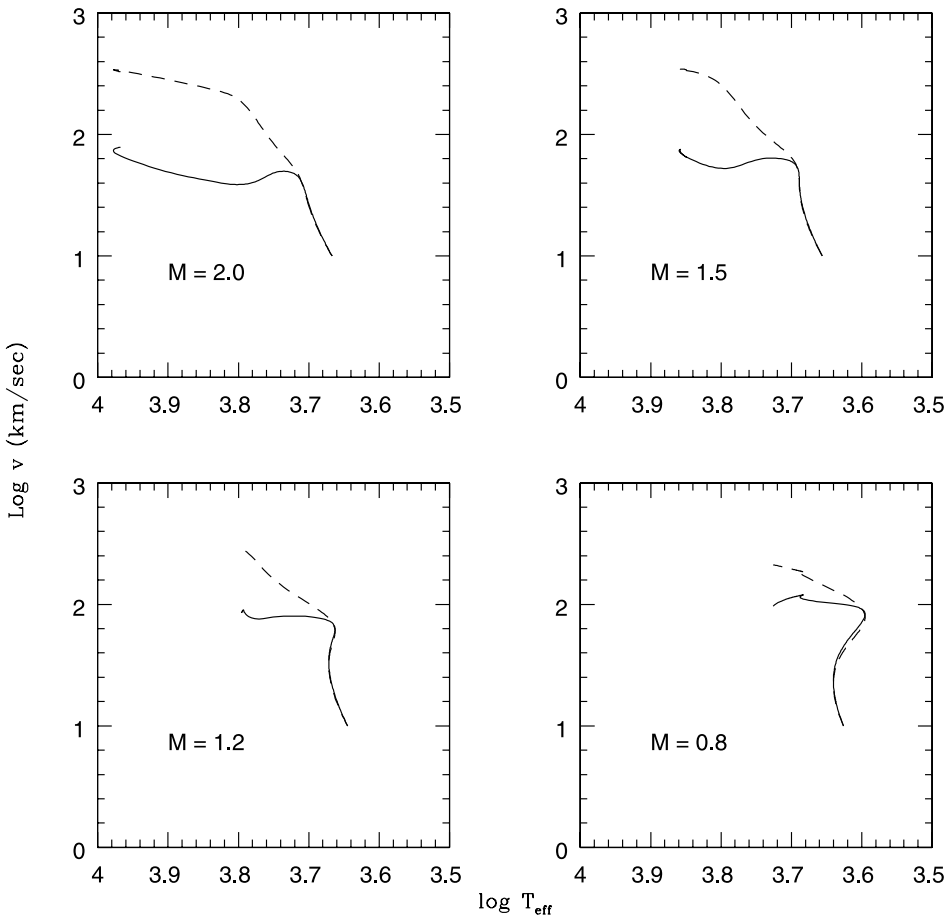

FIG. 5.—Changes from an assumed starting rotation of 10 km s^{-1} predicted by the SFRI models on the assumptions that (1) there is no radial exchange of angular momentum and angular momentum is conserved in shells (*solid lines*) and (2) stars rotate as solid bodies (*dashed lines*). The results are shown for four different masses. The stars initially evolve at nearly constant $T_{\rm eff}$ toward higher rotational velocities as they evolve down their convective tracks. The transition from convective to radiative tracks coincides with the transition from evolution at nearly constant temperature to evolution toward higher temperatures but with relatively small changes in rotation. These calculations terminate when the stars reach the ZAMS. Note that the predictions of the two models are essentially identical for stars evolving along convective tracks. For the two higher mass models, the tracks are nearly parallel once the stars become fully radiative at about $\log T_{\rm eff} = 3.8$, meaning that the fractional spin-up is the same for the two cases along radiative tracks. However, the spin-up predicted for solid-body rotation during the transition from the convective to the radiative tracks is much larger than observed.

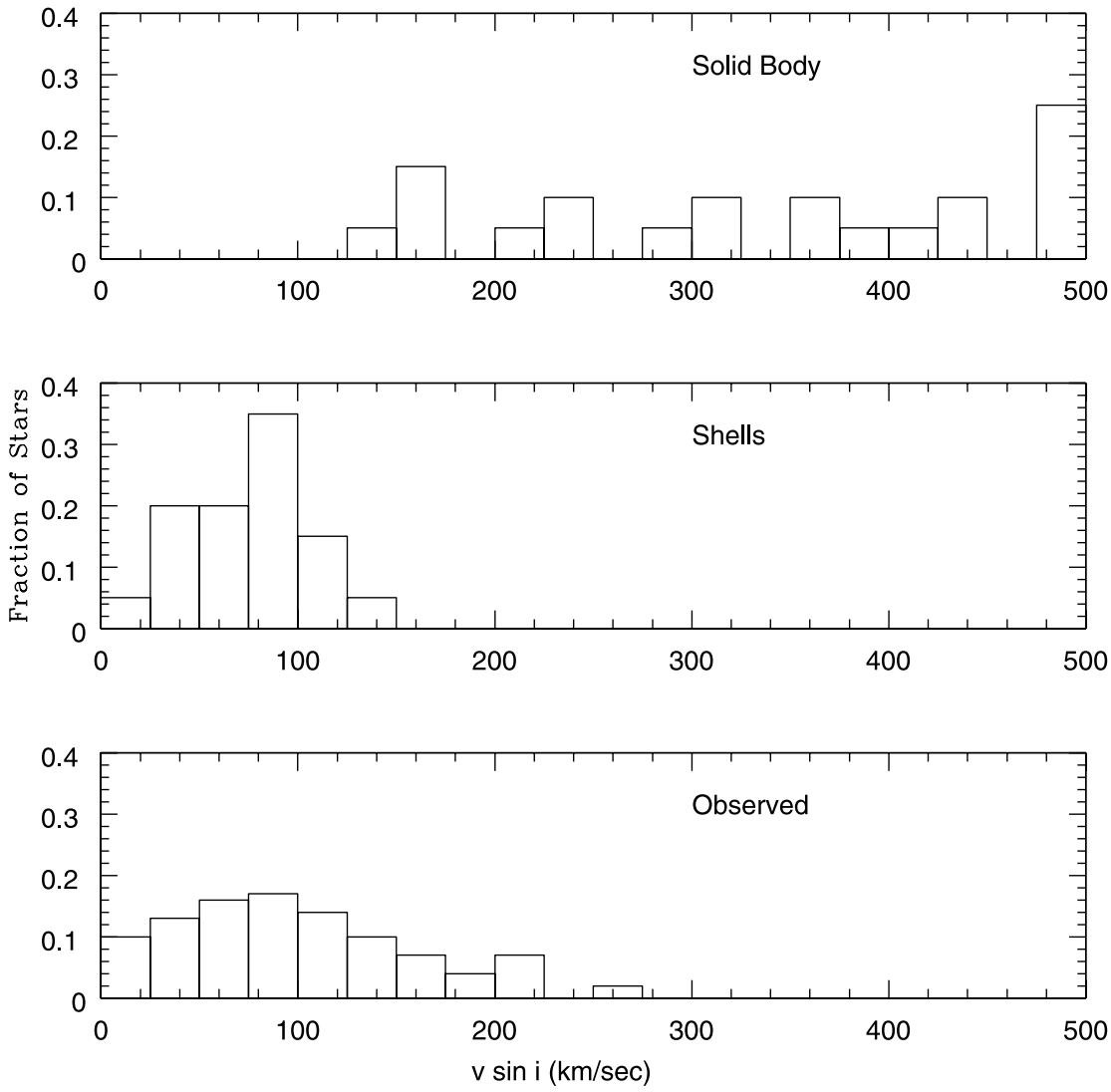

FIG. 6.—Observed and predicted ZAMS rotational velocities. *Top:* Velocities expected on the ZAMS if the 20 stars on convective tracks in the current sample with $M > 1.3\ M_{\odot}$ conserve angular momentum as solid bodies during their subsequent evolution to the main sequence. All of the stars predicted to have rotations in excess of 500 km s^{-1} are plotted in the rightmost box. *Middle:* Predicted velocities if angular momentum is conserved in shells. *Bottom:* Actual velocities for 69 field stars close to the ZAMS with masses in the range 1.5–2 $M_{\odot}$, taken from the study of Wolff & Simon (1997).

cases yield nearly parallel tracks in this logarithmic plot (or for the lowest mass case, predict a relatively small change in surface rotation). Therefore, observations of samples comprising either fully radiative or fully convective stars alone cannot be used to determine empirically how angular momentum is conserved. In fact, either assumption (solid-body rotation or conservation of angular momentum in shells) can be used to predict how the surface rotation will change either *along* radiative or *along* convective tracks. Because of the simplicity of the calculation, we will assume that angular momentum varies inversely with radius along both convective and radiative tracks.

The situation is very different during the *transition* from convective to radiative tracks. It is at this point in its evolution that a star begins to develop a highly concentrated radiative core, and this core can in principle store much of the initial stellar angular momentum. Therefore, it is during this transition that major differences develop in the predicted *surface rotation* rates, depending on how angular momentum is conserved. If the star were to rotate as a solid body during this phase of evolution, the rotation rate would increase by a factor of 4 or more relative to the rate observed on the convective track (cf. Fig. 5).

The observed increase, however, is less than a factor of 4. In our own sample, there are 21 stars on convective tracks with masses greater than 1.2 $M_{\odot}$, and for these stars $\langle v \sin i \rangle = 32 \pm 3$ km s^{-1}. There are 11 stars in this mass range with $3.775 < \log T_{\rm eff} < 3.826$, i.e., at the beginning of their radiative tracks. For these 11 stars, $\langle v \sin i \rangle = 65 \pm 14$ km s^{-1}. The observed spin-up is only a factor of 2 or so, much smaller than predicted for solid-body rotation. Most of the convective stars have $\log T_{\rm eff}$ in the range 3.65–3.70, and reference to Figure 5 shows that if angular momentum is conserved in shells, the spin-up as stars evolve from this temperature range to $\log T_{\rm eff} = \sim 3.8$ is about a factor of 2 for stars with $M > 1.2\ M_{\odot}$, in agreement with the observations.

Therefore, we conclude that "core-envelope decoupling" occurs as PMS stars evolve from convective to radiative tracks. That is, stars that start their post–birth line evolution along convective tracks develop rapidly rotating radiative

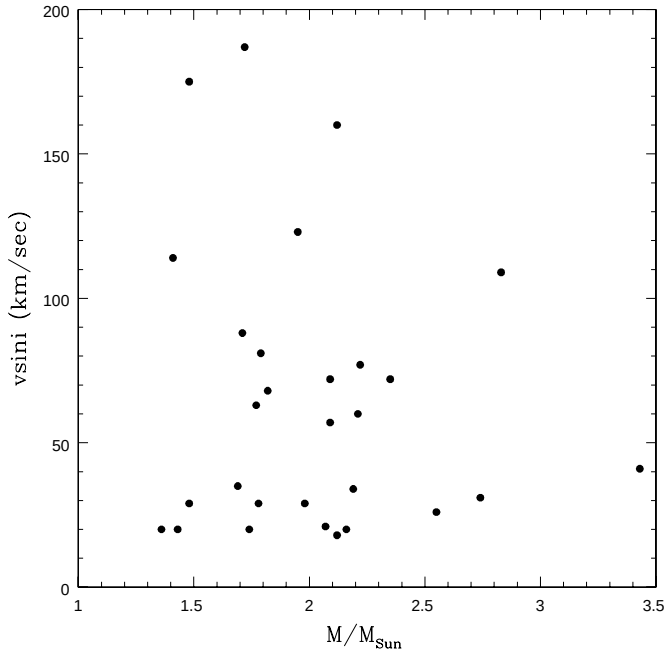

FIG. 7.—Apparent rotational velocities as a function of mass for stars in the temperature range $3.75 < \log T_{\rm eff} < 3.85$. All of these stars are on PMS radiative tracks (see Figs. 2 and 5).

cores and slowly rotating envelopes as they transition from PMS convective to radiative tracks. A number of studies of stars with mass of 1 $M_\odot$ and lower have also concluded that core-envelope decoupling must occur at some point during PMS evolution. These papers have addressed the question of why there are a large number of slowly rotating stars with masses near 1 $M_\odot$ in young clusters and have argued that core-envelope decoupling provides the best explanation (e.g., Krishnamurthi et al. 1997; Allain 1998; Barnes, Sofia, & Pinsonneault 2001; Soderblom, Jones, & Fischer 2001). Our observations of PMS stars that span the transition from convective to radiative phases provide direct confirmation of these inferences, but as we shall see in the next section, core-envelope decoupling accounts for only part of the loss of angular momentum that occurs between the birth line and the main sequence.

6. COMPARISON OF PREDICTED AND OBSERVED ZAMS ROTATIONAL VELOCITIES

6.1. *Stars on PMS Convective Tracks*

The preceding discussion argues that stars evolving from convective to radiative PMS tracks develop rapidly rotating cores and decoupled, slowly rotating envelopes. We expect that changes in observed surface rotation will therefore track the changes in stellar radius. We can check this conclusion by predicting the rotation rates that stars in our sample on convective tracks will have when they reach the ZAMS. The average mass of the stars on convective tracks in our sample is 1.74 $M_\odot$. A good comparison sample is the group of stars closest to the ZAMS with masses in the range 1.5–2 $M_\odot$ studied by Wolff & Simon (1997). In order to predict the rotation rates that the PMS Orion stars will have when they reach the ZAMS, we have used SFRI models to obtain both the ZAMS radii and the moments of inertia as a function of mass. Figure 6 shows the results, in which we have predicted the ZAMS rotation rates for conservation of angular momentum in shells (that is, assuming core-envelope decoupling) and for solid-body rotation. We see that the assumption of solid-body rotation produces a ZAMS distribution that, as anticipated from the above discussion, has essentially no overlap with what is observed for field stars. There is, however, good agreement between the predicted and observed distributions if we assume that the rotation rate varies inversely with stellar radius as expected for core-envelope decoupling.

6.2. *Stars on Radiative Tracks*

We have identified no mechanisms that would cause loss of angular momentum after stars reach $\log T_{\rm eff} = 3.8$ as they evolve toward hotter temperatures and smaller radii. These stars should therefore conserve angular momentum as they complete their evolution to the main sequence. In order to check this prediction, we will take as our initial condition the range of $v \sin i$ values observed for stars with temperatures in the range $\log T_{\rm eff} = 3.75$–3.85. Note that this temperature range encompasses the region of the H-R diagram within

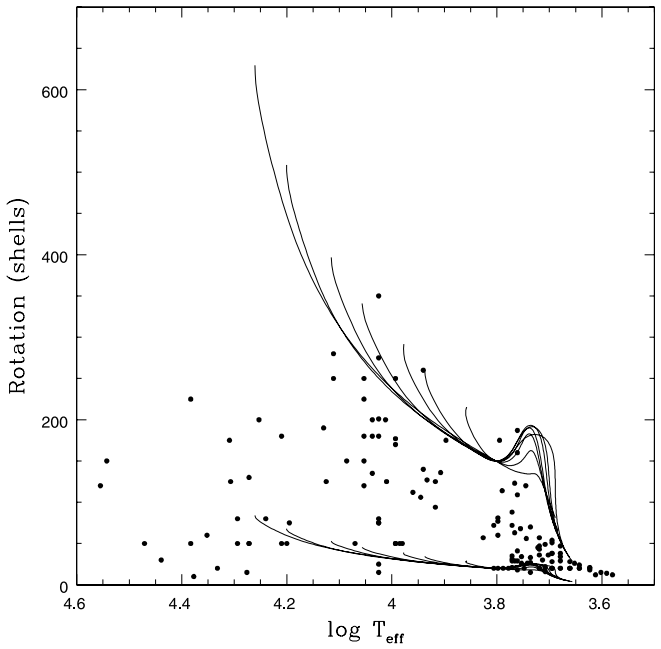

FIG. 8.—Change in rotation predicted by the SFRI models on the assumption that angular momentum is conserved in shells. The lower set of curves is for a rotation rate of 20 km s^{-1} at $\log T_{\rm eff} = 3.8$, where the stars become fully radiative; the upper set is for a rotation rate of 150 km s^{-1} at $\log T_{\rm eff} = 3.8$. The solid lines in each set of curves represent masses of 1.5, 1.8, 2, 2.5, 3, 4, and 5 $M_\odot$. These curves terminate when the stars reach the ZAMS. Filled circles represent data for the Orion stars in Table 2. Up to $\log T_{\rm eff} = 4.1$, nearly all of the stars fall between the two sets of curves and rotation increases systematically with mass. This trend results from the fact that more massive stars traverse longer radiative tracks, contract more, and hence spin up more by the time they reach the main sequence. The trend breaks down, however, for stars with $\log T_{\rm eff} > 4.1$ or masses larger than about 3 $M_\odot$. The maximum observed velocities for these more massive stars lie well below the values predicted if we assume that the stars traverse the full radiative track from $T_{\rm eff} = 3.8$ to the ZAMS. The probable explanation is that the birth line for masses greater than 3.5 $M_\odot$ for the models chosen here crosses the radiative portion of the evolutionary tracks. The distance traversed along radiative tracks from the birth line to the ZAMS, and hence the amount of spin-up, decreases with increasing mass for masses greater than 3.5 $M_\odot$. We have also projected the predictions of $v \sin i$ backward to the convective phase, again on the assumption that angular momentum is conserved in shells. The fact that the convective PMS stars fall within the bands so derived is another indication that the assumption that angular momentum is conserved in shells provides a good description of the data.

which stars of masses 1.5–3.5 $M_\odot$ transition from convective to radiative tracks. The data in Table 2 show that the Orion stars reach this temperature with a range of rotation rates from less than 20 km s^{-1} to nearly 200 km s^{-1}, with the majority of stars having rotations less than 150 km s^{-1} (see Fig. 7). In accord with our previous discussion, we will assume that the rotation rates of these stars then vary inversely with the radius (see also Hartmann et al. 1986).

In Figure 8 we have plotted the predicted changes in $v \sin i$ as stars evolve along radiative tracks to the main sequence. This figure illustrates several points. First, the rotational velocities of most of the stars in the current sample lie between the bands defined by evolving models for initial values of $v \sin i$ equal to 20 and 150 km s^{-1}. Therefore, the *range* of rotational velocities observed at the end point of the contraction, namely, along the ZAMS, is fully consistent with the *range* seen among PMS stars. Hence, as expected, there is no evidence for significant loss of angular momentum along radiative tracks. Second, on the basis of these simple models we would expect $v \sin i$ on average to increase with increasing mass because more massive stars contract more as they traverse their longer radiative tracks, and this expectation is consistent with the observations up to about 3 $M_\odot$.

Figure 8 shows that the prediction that rotation will continue to increase to values in excess of 400 km s^{-1} for stars with masses greater than 4 $M_\odot$ is not borne out by the observations. While our sample is small, this conclusion is supported by much larger surveys (e.g., Abt et al. 2002; Wolff, Edwards, & Preston 1982). This result has a natural explanation in terms of the birth line. Stars with masses greater than 3.5 $M_\odot$, given our particular choice of models, are already on radiative tracks when accretion stops. The portion of the radiative track that they traverse decreases with increasing mass, and the corresponding spin-up from the initial conditions when they are released at the birth line will also decrease, thereby limiting the maximum observed rotational velocity.

6.3. *The Break in the Power Law*

We now turn to an explanation of why J/M decreases sharply with M for stars with masses less than about 2 $M_\odot$ that have completed the convective phase of evolution. We have noted already that core-envelope decoupling during the transition from convective to radiative tracks will account for some apparent loss of observed surface angular momentum. Core-envelope decoupling cannot, however, account for the sharp downturn in J/M. The effects of core-envelope decoupling are predicted to be largest for stars around 2 $M_\odot$ and to diminish toward lower masses (see Fig. 5). This prediction is in the opposite sense to the trend seen in the observations: the differences between the angular momenta of stars on convective tracks and the values for stars on radiative tracks (compare Figs. 3*a* and 3*b*) are much larger at 1 $M_\odot$ than at 2 $M_\odot$.

An additional mechanism is apparently required to explain the observations, and we suggest that this mechanism is braking while stars with $M < 2\ M_\odot$ evolve down their convective tracks. Stars on convective tracks have accretion rates on the order of $10^{-8}\ M_\odot\ \mathrm{yr}^{-1}$ (e.g., Valenti, Basri, & Johns 1993; Gullbring et al. 1998). If these stars are locked to their disks, then the disks could in principle act as a brake and cause additional loss of angular momentum.

Hartmann (2002) has pointed out that three factors will determine the amount of spin-down for a PMS star: (1) the time spent on the convective track, (2) the timescale for disk braking, and (3) the lifetime of the disk. He has estimated that the disk-braking timescale is given by

$$\tau_{\mathrm{DB}} = 4.5 \times 10^6\ \mathrm{yr} \left(\frac{M}{0.5\ M_\odot}\right)\left(\frac{10^{-8}\ M_\odot\ \mathrm{yr}^{-1}}{\dot{M}}\right) f, \quad (7)$$

where the mass and accretion rate parameters are scaled to values typical of low-mass T Tauri stars (Gullbring et al. 1998; Hartmann et al. 1998) and f is the ratio of the actual velocity to the breakup velocity. We will take, following Hartmann (see also Fig. 3*a*), $f = 0.2$. We can then calculate the ratio of τ_{DB} to the time a contracting star spends moving down the convective track from the birth line to the transition to the radiative track, after which we expect braking to be minimal because of the absence of magnetic fields. In order to estimate the convective lifetime, we have used the SFRI models to determine the time that elapses as a star moves from the PS birth line to the bottom of the convective track.

The results are shown in Figure 9. The shape of this curve mimics the shape of the relationship between J/M and mass for PMS Orion stars on radiative tracks. The lower the mass of a star, the longer the time it spends evolving down its convective track and the more angular momentum it can lose, provided of course that the disk lifetime is also long enough. Stars with masses close to 2 $M_\odot$ enter the radiative phase before disks can remove significant stellar angular momentum. Therefore, braking on the convective track provides a very natural explanation for the break in the power law seen for post–convective track stars with $M < 2\ M_\odot$. Analysis of data for Orion and several hundred other PMS stars with masses in the range 0.5–1 $M_\odot$ shows that these stars on average reduce their rotational velocities by about a factor of 3 while contracting by about a factor of 3 as they evolve down convective tracks, thereby reducing their angular momentum by about an order of magnitude (Rebull et al. 2002; Rebull, Wolff, & Strom 2004).

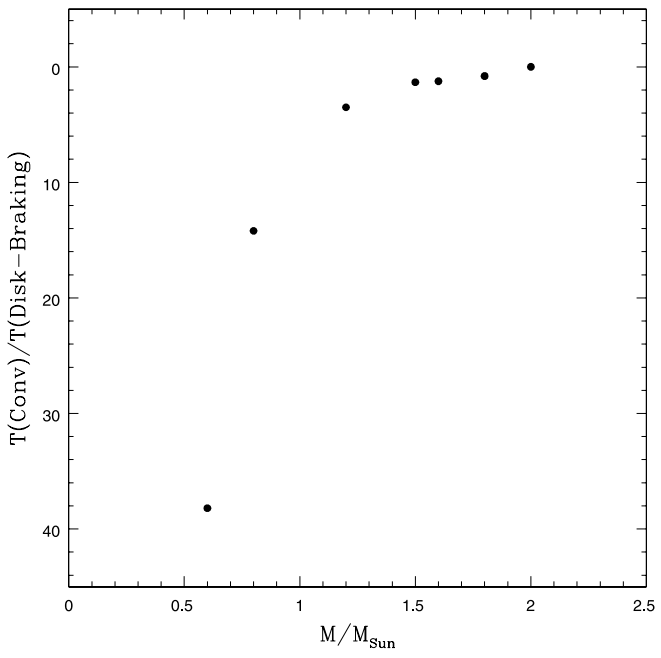

FIG. 9.—Ratio of the time spent on the convective track to the timescale for disk braking estimated by the formulation of Hartmann (2002). Stars with masses close to 2 $M_\odot$ evolve too rapidly to shed much angular momentum during this phase of evolution.

Quantitatively, this is just what is required in order to account for the break in the J/M power law (see Fig. 3*b*).

7. CONCLUSIONS

We have presented new measurements of rotational velocities for a sample of stars with masses in the range 0.4–14 $M_\odot$ (median mass 2.1 $M_\odot$) and considered literature data for stars of less than 0.5 $M_\odot$. Observations of the youngest stars in Orion show that the specific angular momentum of stars on *convective* tracks increases slowly and continuously with stellar mass over the mass range from 0.1 $M_\odot$ to nearly 3 $M_\odot$ and merges smoothly with the J/M versus M relationship for young main-sequence stars with masses between 3 and 10 $M_\odot$. The power-law relationship between J/M and M for newly formed stars suggests a common mechanism for establishing J/M throughout this entire range, which spans a factor of 100 in mass. The power-law relationship between J/M and M for convective PMS stars differs significantly from what is observed for both older PMS stars, which have evolved from convective to radiative tracks, and main-sequence stars. For these older stars, J/M follows the same power-law relationship as the convective stars for $M > 2\ M_\odot$ but decreases sharply with decreasing mass for stars with $M < 2\ M_\odot$.

These observations establish the basic trends in angular momentum as a function of time and mass that models must explain. Comparison with very simple models shows that these overall trends can be explained by five distinct processes that are effective at different stages of evolution: (1) an angular momentum loss process, possibly disk locking, that operates before stars reach the birth line and applies to all stars with masses between 0.1 and 10 $M_\odot$; (2) braking of stars with $M < 2\ M_\odot$ as they evolve down their convective tracks, with the amount of braking increasing with time spent in this phase of evolution and hence with decreasing mass; (3) decoupling of the angular momentum seen at the surface of the star from the angular momentum in the interior when stars with $M < 2$–$4\ M_\odot$ make the transition from convective to radiative PMS evolution; (4) conservation of angular momentum as stars evolve along their radiative tracks; and (5) additional spin-down by magnetic winds of stars with $M < 1.4\ M_\odot$ after these stars reach the main sequence.

While much more sophisticated models may eventually be required to explain the trends observed here, these results show the potential power of observations of stellar rotation as probes of fundamental processes that occur during the formation and early evolution of stars.

REFERENCES

Abt, H. A., & Hunter, J. H. 1962, ApJ, 136, 381
Abt, H. A., Levato, H., & Grosso, M. 2002, ApJ, 573, 359
Abt, H. A., & Morrell, N. I. 1995, ApJS, 99, 135
Abt, H. A., Muncaster, G. W., & Thompson, L. A. 1970, AJ, 75, 1095
Allain, S. 1998, A&A, 333, 629
Anderson, C. M., Stoeckly, R., & Kraft, R. P. 1966, ApJ, 143, 299
Barnes, S., Sofia, S., & Pinsonneault, M. 2001, ApJ, 548, 1071
Behrend, R., & Maeder, A. 2001, A&A, 373, 190
Bessell, M. S. 1991, AJ, 101, 662
Brown, A. G. A., de Geus, E. J., & de Zeeuw, P. T. 1994, A&A, 289, 101
Brun, A. 1935, Publ. Obs. Lyon, 1, 12
Chandrasekhar, S., & Munch, G. 1950, ApJ, 111, 142
Chlebowski, T., & Garmany, C. D. 1991, ApJ, 368, 241
Code, A. D., Bless, R. C., Davis, J., & Brown, R. H. 1976, ApJ, 203, 417
Cohen, M., & Kuhi, L. V. 1979, ApJS, 41, 743
Conti, P. S., & Ebbets, D. 1977, 213, 438
Cox, A. N., ed. 2000, Allen's Astrophysical Quantities (4th ed.; New York: AIP)
Duncan, D. 1993, ApJ, 406, 172
Durisen, R. H., Yang, S., Cassen, P., & Stahler, S. W. 1989, ApJ, 345, 959
Edwards, S., et al. 1993, AJ, 106, 372
Elias, J. H., Frogel, J. A., Matthews, K., & Neugebauer, G. 1982, AJ, 87, 1029
Feigelson, E. D., Broos, P., Gaffney, J. A., Garmire, G., Hillenbrand, L. A., Pravdo, S. H., Townsley, L., & Tsuboi, Y. 2002, ApJ, 574, 258
Feigelson, E. D., Gaffney, J. A., Garmire, G., Hillenbrand, L. A., & Townsley, L. 2003, ApJ, 584, 911
Flaccomio, E., Damiani, F., Micela, G., Sciortino, S., Harnden, F. R., Murray, S. S., & Wolk, S. J. 2003, ApJ, 582, 398
Gagne, J., Caillault, J.-P., & Stauffer, J. R. 1995, ApJ, 445, 280
Genzel, R., & Stutzki, J. 1989, ARA&A, 27, 41
Guenther, E. W., Lehmann, H., Emerson, J. P., & Staude, J. 1999, A&A, 341, 768
Gullbring, E., Hartmann, L., Briceno, C., & Calvet, N. 1998, ApJ, 492, 323
Hartmann, L. 2002, ApJ, 566, L29
Hartmann, L., Calvet, N., Gullbring, E., & D'Alessio, P. 1998, ApJ, 495, 385
Hartmann, L., Hewett, R., Stahler, S., & Mathieu, R. D. 1986, ApJ, 309, 275
Herbst, W., Bailer-Jones, C. A. L., & Mundt, R. 2001, ApJ, 554, L197
Hillenbrand, L. A. 1997, AJ, 113, 1733
Hillenbrand, L. A., Strom, S. E., Calvet, N., Merrill, K. M., Gatley, I., Makidon, R. B., Meyer, M. R., & Skrutskie, M. F. 1998, AJ, 116, 1816
Hillenbrand, L. A., Strom, S. E., Vrba, F. J., & Keene, J. 1992, ApJ, 397, 613
Humphreys, R. M., & McElroy, D. B. 1984, ApJ, 284, 565
Johns-Krull, C. M., & Gafford, A. D. 2002, ApJ, 573, 685
Johns-Krull, C. M., Valenti, J. A., & Koresko, C. 1999, ApJ, 516, 900
Johnson, H. L. 1966, ARA&A, 4, 193
Jones, B. F., & Walker, M. F. 1988, AJ, 95, 1755
Kawaler, S. D. 1987, PASP, 99, 1322
Kenyon, S. J. 1988, AJ, 96, 337
Königl, A. 1991, ApJ, 370, L39
Kraft, R. P. 1970, in Spectroscopic Astrophysics, ed. G. H. Herbig (Berkeley: Univ. California Press), 385
Krishnamurthi, A., Pinsonneault, M. H., Barnes, S., & Sofia, S. 1997, ApJ, 480, 303
MacGregor, K. B., & Charbonneau, P. 1994, in ASP Conf. Ser. 64, Cool Stars, Stellar Systems, and the Sun, Eighth Cambridge Workshop, ed. J.-P. Caillaut (San Francisco: ASP), 174
Maeder, A., & Meynet, G. 1988, A&AS, 76, 411
Massey, P., Parker, J. W., & Garmany, C. D. 1989, AJ, 98, 1305
Mathieu, R. D., Ghez, A. M., Jensen, E. L. N., & Simon, M. 2000, in Protostars and Planets IV, ed. V. Mannings, A. Boss, & S. S. Russell (Tucson: Univ. Arizona Press), 703
McNamara, B. J. 1976, AJ, 81, 845
McNamara, B. J., Hack, W. J., Olson, R. W., & Mathieu, R. D. 1989, AJ, 97, 1427
McNamara, D. H. 1963, ApJ, 137, 316
McNamara, D. H., & Larsson, H. J. 1962, ApJ, 135, 748
Mundt, T., & Bastien, U. 1980, A&AS, 39, 245
Norberg, P., & Maeder, A. 2000, A&A, 359, 1025
Palla, F., & Stahler, S. W. 1992, ApJ, 392, 667
———. 1993, ApJ, 418, 414
Parenago, P. P. 1954, Trudy Sternberg Astron. Inst., 25, 1
Penston, M. V. 1973, ApJ, 183, 505
Penston, M. V., Hunter, J. K., & O'Neill, A. 1975, MNRAS, 171, 219
Rebull, L. M. 2001, AJ, 121, 1676
Rebull, L. M., Wolff, S. C., & Strom, S. E. 2004, AJ, in press
Rebull, L. M., Wolff, S. C., Strom, S. E., & Makidon, R. B. 2002, AJ, 124, 546
Rhode, K. L., Herbst, W., & Mathieu, R. D. 2001, AJ, 122, 3258
Rydgren, A. E., & Vrba, F. J. 1984, AJ, 89, 399
Shu, F., Najita, J., Ostriker, E., Wilkin, F., Ruden, S., & Lizano, S. 1994, ApJ, 429, 781
Slettebak, A., Collins, G. W., II, Parkinson, T. D., Boyce, P. B., & White, N. M. 1975, ApJS, 29, 137
Smith, M. A., Beckers, J. M., & Barden, S. C. 1983, ApJ, 271, 237
Soderblom, D. R., Jones, B. F., & Fischer, D. 2001, ApJ, 563, 334
Soderblom, D. R., Pendleton, J., & Pallavicini, R. 1989, AJ, 97, 539
Stahler, S. W. 1983, ApJ, 274, 822
Stauffer, J. R., & Hartmann, L. W. 1986, PASP, 98, 1233
Swenson, F. J., Faulkner, J., Rogers, F. J., & Iglesias, C. A. 1994, ApJ, 425, 286 (SFRI)
Tonry, J., & Davis, M. 1979, AJ, 84, 1511

Uchida, Y., & Shibata, K. 1984, PASJ, 36, 105
Valenti, J. A., Basri, G., & Johns, C. M. 1993, AJ, 106, 2024
van Altena, W. F., Lee, J. T., Lee, J.-F., Lu, P. K., & Upgren, A. R. 1988, AJ, 95, 1744
Walker, M. F. 1969, ApJ, 155, 447
———. 1983, ApJ, 271, 642
Walker, M. F. 1990, PASP, 102, 726
Warren, W. H., & Hesser, J. E. 1977, ApJS, 34, 115
———. 1978, ApJS, 36, 497
Wolff, S. C. 1990, AJ, 100, 1994
Wolff, S. C., Edwards, S., & Preston, G. W. 1982, ApJ, 252, 322
Wolff, S. C., & Simon, T. 1997, PASP, 109, 759